

AD-A098 266

YALE UNIV NEW HAVEN CONN DEPT OF ENGINEERING AND AP--ETC F/G 9/3
FAST SWITCHES FOR OPTICAL COMMUNICATION UTILIZING OPTICAL KERR --ETC(U)
MAR 81 R K CHANG F1962A-78-C-0021

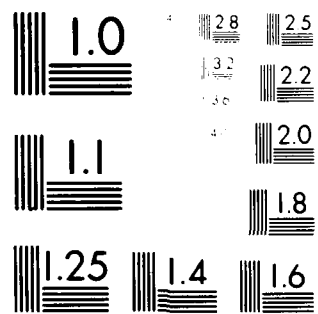
UNCLASSIFIED

RADC-TR-80-87

NL

1 03 1
AD-A
0-102-10

END
DATE
FILMED
5-81
DTIC



MICROCOPY RESOLUTION TEST CHART
 NATIONAL BUREAU OF STANDARDS-1963-A

TW

RADC-TR-80-87
Final Technical Report
March 1981

LEVEL

12



FAST SWITCHES FOR OPTICAL COMMUNICATION UTILIZING OPTICAL KERR OR ELLIPSE ROTATION EFFECT

Yale University

Richard K. Chang

DTIC
ELECTRONICS
APR 28 1981

APPROVED FOR PUBLIC RELEASE; DISTRIBUTION UNLIMITED

This research was supported by the Laboratory Director's Fund.

AD A 098268

DTIC FILE COPY

ROME AIR DEVELOPMENT CENTER
Air Force Systems Command
Griffiss Air Force Base, New York 13441

81 4 27 096

This report has been reviewed by the RADC Public Affairs Office (PA) and is releasable to the National Technical Information Service (NTIS). At NTIS it will be releasable to the general public, including foreign nations.

RADC-TR-80-87 has been reviewed and is approved for publication.

APPROVED:



BERNARD BENDOW
Project Engineer

APPROVED:



CLARENCE D. TURNER
Acting Director
Solid State Sciences Division

FOR THE COMMANDER:



JOHN P. HUSS
Acting Chief, Plans Office

If your address has changed or if you wish to be removed from the RADC mailing list, or if the addressee is no longer employed by your organization, please notify RADC (ESO) Hanscom AFB MA 01731. This will assist us in maintaining a current mailing list.

Do not return this copy. Retain or destroy.

UNCLASSIFIED

SECURITY CLASSIFICATION OF THIS PAGE (When Data Entered)

(19) REPORT DOCUMENTATION PAGE		READ INSTRUCTIONS BEFORE COMPLETING FORM
1. REPORT NUMBER RADC-TR-80-87	2. GOVT ACCESSION NO. AD-A098 2.68	3. RECIPIENT'S CATALOG NUMBER
4. TITLE (and Subtitle) FAST SWITCHES FOR OPTICAL COMMUNICATION UTILIZING OPTICAL KERR OR ELLIPSE ROTATION EFFECT.	5. TYPE OF REPORT & PERIOD COVERED Final Technical Report 1 Oct 77 - 30 Sep 79	6. PERFORMING ORG. REPORT NUMBER N/A
7. AUTHOR(s) Richard K. Chang	8. CONTRACT OR GRANT NUMBER(s) F19628-78-C-0021	
9. PERFORMING ORGANIZATION NAME AND ADDRESS Yale University Dept of Engineering and Applied Science New Haven CT 06520	10. PROGRAM ELEMENT, PROJECT, TASK AREA & WORK UNIT NUMBERS 61101F 01707820	
11. CONTROLLING OFFICE NAME AND ADDRESS Deputy for Electronic Technology (RADC/ESO) Hanscom AFB MA 01731	12. REPORT DATE March 1981	13. NUMBER OF PAGES 67
14. MONITORING AGENCY NAME & ADDRESS (if different from Controlling Office) Same	15. SECURITY CLASS. (of this report) UNCLASSIFIED	15a. DECLASSIFICATION/DOWNGRADING SCHEDULE N/A
16. DISTRIBUTION STATEMENT (of this Report) Approved for public release; distribution unlimited.		
17. DISTRIBUTION STATEMENT (of the abstract entered in Block 20, if different from Report) Same		
18. SUPPLEMENTARY NOTES RADC Project Engineer: Dr. Bernard Bendow (ESO) This research was supported by the Laboratory Director's Fund.		
19. KEY WORDS (Continue on reverse side if necessary and identify by block number) Nonlinear absorption Optically induced refractive Third-order nonlinear optical effects index changes Bistability Fabry-Perot interferometer Optically activated light switches Photorefractive effect		
20. ABSTRACT (Continue on reverse side if necessary and identify by block number) This report summarizes the results of an investigation of several different types of optically activated light switches based on third-order nonlinear optical effects. Two optical switches utilizing the change of refractive index induced in a nonlinear medium by an intense light beam are described: one utilizes a single-pass and the other a multiple-pass (interferometric) geometry. Results of a search to find new media with large nonlinearities are given, and the possibility of		

DD FORM 1 JAN 73 1473 EDITION OF 1 NOV 69 IS OBSOLETE

UNCLASSIFIED
SECURITY CLASSIFICATION OF THIS PAGE (When Data Entered)

UNCLASSIFIED

SECURITY CLASSIFICATION OF THIS PAGE(When Data Entered)

increasing the nonlinearity of commonly used media by Raman-type resonant enhancement is discussed. The theoretical and experimental behavior of a Fabry-Perot interferometer switch with a nonlinearly absorbing intracavity medium is also presented. In some cases, the switch could be activated by anomalously low pump powers, and possible mechanisms for this effect are discussed.

The results of a literature search on the photorefractive effect are presented along with the results of an experimental effort to measure the photorefractive effect in Ge:SiO_2 .

UNCLASSIFIED

SECURITY CLASSIFICATION OF THIS PAGE(When Data Entered)

TABLE OF CONTENTS

	Page
I. Introduction	1
II. Optical Kerr Effect Switch	3
III. Fabry-Perot Interferometer Switch - Nonlinear Index	7
IV. Third-Order Nonlinear Susceptibility	14
A. $\chi^{(3)}$ in Liquids and Solids	14
B. Resonant Enhancement of $\chi^{(3)}$	19
V. Fabry-Perot Interferometer Switch - Nonlinear Absorption	24
A. Intracavity Excited-State Absorber	31
B. Intracavity Two-Photon Absorber	42
C. Discussion of Experimental Results - Induced Index Change	49
VI. The Photorefractive Effect	55
References	58
Appendix A, Bibliography on the Photorefractive Effect	61

Accession For	
NTIS GRA&I	<input checked="checked" type="checkbox"/>
DTIC TAB	<input type="checkbox"/>
Unannounced	<input type="checkbox"/>
Justification	
By _____	
Distribution/	
Availability Codes	
Dist	Avail and/or Special
A	

EVALUATION

The report has been useful in indicating the possibility of optically activated switching using semiconducting crystals in a Fabry-Perot cavity. This design may eventually contribute to fast switching components for C^3 fiber optics systems related to TPO 3B.



BERNARD BENDOW
Project Engineer

I. INTRODUCTION

The purpose of this work was to investigate the applicability of third-order nonlinear optical effects to the problem of making light-activated optical switches for fiber optics communications. The first two sections of this report describe two optical switches based on the change of refractive index induced in a nonlinear medium by an intense light beam: in the first type of switch, the index change is probed by a signal beam in a single-pass configuration; and in the second switch, a resonant Fabry-Perot interferometer is used to enhance the signal beam sensitivity to the induced index change.

An inherent difficulty with third-order nonlinear effects is that they are generally observable only with relatively intense optical fields which are incompatible with integrated and fiber optics. In the third section of the report we therefore discuss our efforts toward finding nonlinear liquid and solid media with large nonlinear susceptibilities in an effort to reduce the pump beam power required in the switches outlined above. The fourth section considers the possibility of enhancing the nonlinear susceptibility by tuning the pump and signal beams to a Raman resonance of the nonlinear medium.

An interferometer can also be used to enhance the signal beam sensitivity to nonlinear absorption induced by a pump beam, and in the fifth section of the report we discuss the behavior of a Fabry-Perot interferometer with intracavity excited-state or two-photon absorbers. In our experimental investigation of such a device, using filter glass as the excited-state absorber and CdS as the two-photon absorber, we

discovered that the interferometer switch could be activated by anomalously low pump powers due to an induced index change in the medium. Two possible mechanisms for this effect are discussed.

Finally, we present the results of our literature search to find photorefractive materials and describe our experimental efforts to observe the effect in a material reported to be photorefractive.

II. OPTICAL KERR EFFECT SWITCH

The optical Kerr effect¹ is a nonlinear optical effect involving the third-order susceptibility $\chi^{(3)}$, in which a strong optical frequency electric field induces optical birefringence in a normally isotropic medium. This effect is usually observed experimentally by probing the birefringence induced by the strong, linearly polarized pump beam at frequency ω_p with a weaker signal beam at frequency ω_s linearly polarized at some angle γ to the pump polarization. In the absence of the pump beam, the signal beam is blocked by an analyzing polarizer, but when the pump beam is present, the induced birefringence in the nonlinear medium causes the signal beam to become elliptically polarized, thus allowing some portion of it to pass through the analyzer (see Fig. 1). The application of this effect as a switch is straightforward, as the signal beam can be switched back and forth between the 'reject' and 'pass' ports of the analyzer by turning the pump beam on and off.

For a linearly polarized pump beam, one defines two birefringent axes parallel and perpendicular to the electric field of the pump. The signal beam polarization is then resolved along these axes, and the difference in refractive index Δ observed by the two polarization components is²

$$\begin{aligned}\Delta &= \delta n_{||} - \delta n_{\perp} \\ &= \frac{2\pi}{n} \chi^{(3)} |E_{\text{pump}}|^2\end{aligned}$$

where n = linear refractive index of the medium, and $\delta n_{||}$ and δn_{\perp} refer to induced index changes parallel and perpendicular to the pump polarization,

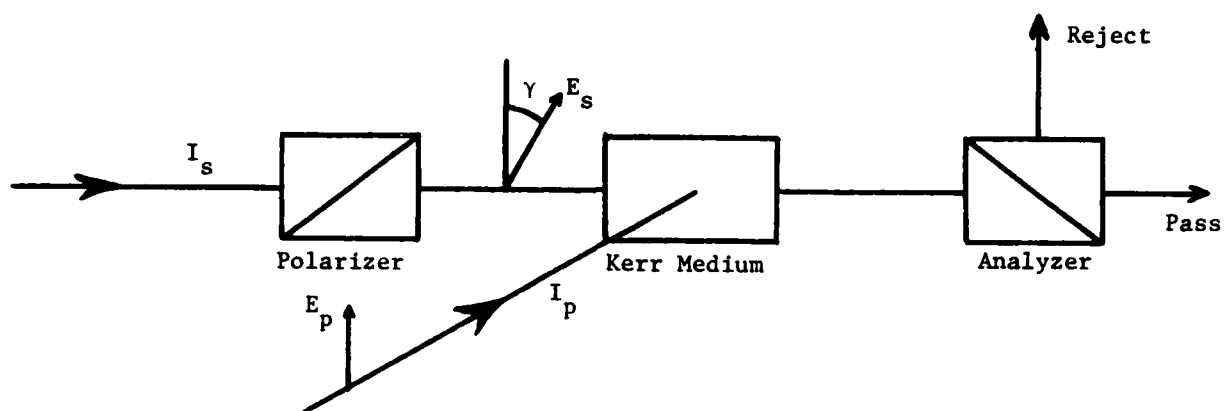


FIGURE 1. An optical Kerr effect shutter. In the absence of the strong pump (I_p), the signal beam (I_s) exits from the reject port of the analyzer; when the pump beam is present, part of the signal beam is switched to the pass port.

respectively. The exact form of the nonlinear susceptibility $\chi^{(3)}$ depends on the symmetry of the medium and on the frequencies ω_p and ω_s . The phase shift induced between the two polarization components of the signal beam after traversing pathlength ℓ through the medium is

$$\phi = \frac{2\pi\ell}{\lambda_s} \Delta$$

$$\approx \pi \ell B |E_{\text{pump}}|^2$$

where λ_s = wavelength of the signal beam and $B = 2\omega_s \chi^{(3)}/nc$, the optical Kerr coefficient. With the signal and pump polarizations at 45° to one another ($\gamma = \pi/4$), the transmission through the analyzer is

$$T = \sin^2 (\phi/2) .$$

The pump intensity required to activate this switch can be calculated using the known nonlinear susceptibilities of two highly nonlinear liquids, CS_2 and the nematic liquid crystal MBBA. Their optical Kerr coefficients are^{3,4}

$$B_{\text{CS}_2} = 3.5 \times 10^{-7} \text{ cm}^2/\text{erg}$$

$$B_{\text{MBBA}} = 2.9 \times 10^{-6} \text{ cm}^2/\text{erg} \quad (\text{at } 53^\circ\text{C}).$$

The pump intensities required to induce 75% transmission of the signal beam for a 1 cm pathlength for each material are given in Table 1.

TABLE 1		
Liquid	$B(\text{cm}^2/\text{erg})$	$I(\text{MW}/\text{cm}^2)$
CS_2	3.5×10^{-7}	368
MBBA	2.9×10^{-6}	44

From these intensities it is clear that a device of this type would not be a practical switch. MBBA is impractical because it must be kept at a constant, elevated temperature (just above the nematic to isotropic phase transition) and has a slow response time (~ 50 nsec at 53°C).⁴ Although CS_2 has one of the largest nonlinear coefficients of any liquid, the pump intensity required to induce $T = 75\%$ is so high that other nonlinear effects (e.g., self-focusing, stimulated Raman and Brillouin scattering) will set in and obscure the desired Kerr effect. In the following sections, we will discuss various approaches we have taken in an effort to obtain effective switching action with more manageable pump powers.

III. FABRY-PEROT INTERFEROMETER SWITCH - NONLINEAR INDEX

A more efficient way to take advantage of the intensity dependent refractive index of a nonlinear medium is to place the medium within the cavity of a Fabry-Perot interferometer. When the signal beam is tuned to resonance with the Fabry-Perot cavity it effectively makes many passes through the intracavity medium, thus increasing the path length ℓ , which results in a larger phase shift in the signal than would be obtained in the single-pass Kerr switch due to a given induced index change.

According to the simple plane wave theory of a Fabry-Perot interferometer having perfectly flat and exactly parallel mirrors, the transmission is given by⁵

$$T = \frac{1}{1 + F \sin^2(k\ell)}$$

where

$$F = 4R_m / (1 - R_m)^2$$

R_m = mirror reflectivity

$$k\ell = 2\pi n\ell / \lambda_s$$

λ_s = wavelength of signal beam

ℓ = spacing between mirrors .

For a lossless interferometer, the reflectivity of the etalon is just $R = 1 - T$. If we allow the refractive index of the intracavity medium to be intensity dependent, i.e., $n = n + \delta n_{||}$, we have

$$\frac{2\pi n_0 \ell}{\lambda_s} + \frac{2\pi n_2 \ell}{\lambda_s} |E|^2$$

where

$$n_2 \equiv \delta n / |E|^2 .$$

Thus, it is possible to change the transmission of the interferometer simply by varying the intracavity intensity ($|E|^2$). This device is capable of operating in several different modes (bistable, transistor, limiting) and is discussed in detail in Refs. 6 - 7.

Application of the nonlinear Fabry-Perot etalon as a switch requires two light beams: (1) a weak signal beam (frequency ω_s) in near or exact resonance (high transmission) with the Fabry-Perot cavity, and (2) a strong pump beam (frequency ω_p) that irradiates the nonlinear medium without interacting with the interferometer cavity (see Fig. 2) either because it does not pass through the mirrors or because the mirrors do not reflect light at frequency ω_p . In one possible mode of operation, the cavity is initially tuned (by varying the mirror spacing, ℓ) so that the weak signal beam is just off resonance, i.e., the transmission is low, and the reflectivity is high. The pump beam can then change the index of refraction sufficiently to tune the cavity into resonance with the signal beam, resulting in the signal beam switching from the reflected to transmitted state. Similarly, one could initially tune the cavity to high transmission at ω_s and then have the pump beam switch the etalon to high reflectivity at ω_s .

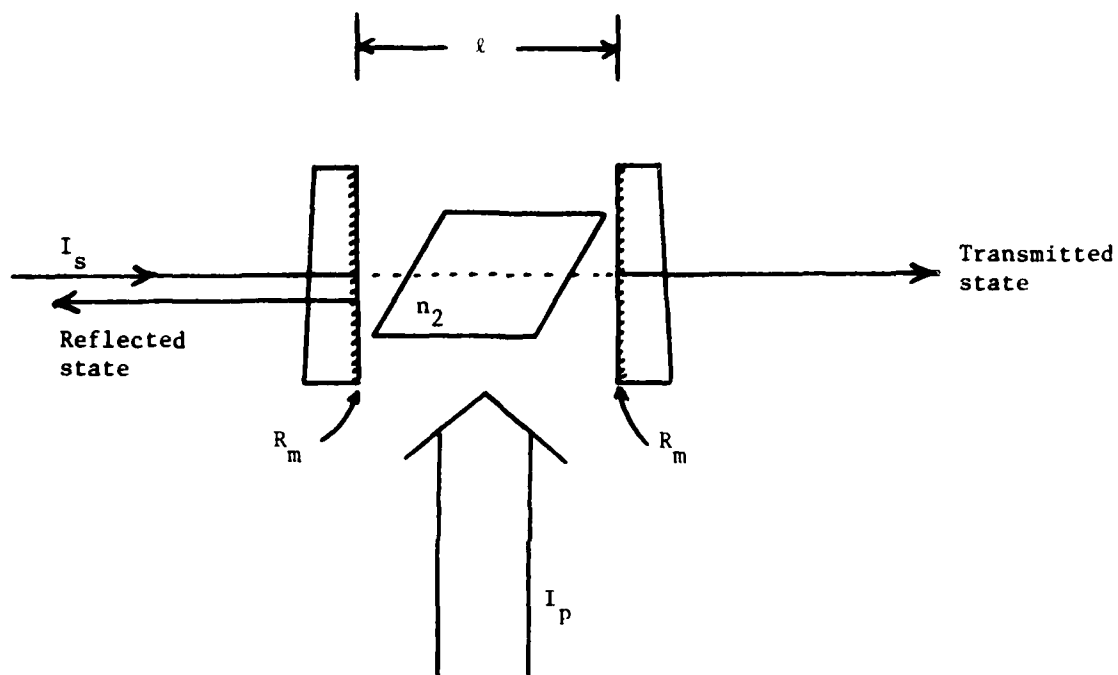


FIGURE 2. The Fabry-Perot interferometer optical switch. The interferometer cavity is defined by the two mirrors of reflectivity R_m at ω_s with spacing l . A pump induced index change in the nonlinear medium (n_2) results in the signal beam being switched between the transmitted and reflected states.

The induced refractive index change responsible for the nonlinear behavior of the interferometer is identical to that responsible for the optical Kerr effect; the only difference is in the way the index change is probed by the signal beam. In the Kerr effect, the pump and signal beams are polarized at 45° to one another, so that the signal sees both $\delta n_{||}$ and δn_{\perp} and thus experiences a change in polarization state. In the nonlinear Fabry-Perot etalon, the signal and pump beam polarizations are parallel to one another, so that the signal sees only a change in the optical path length, due to the induced change in n . The relationship between B and n_2 is given here

$$n_2 = \frac{2\pi}{n} \chi^{(3)} \\ = \frac{\pi c}{\omega_s} B .$$

The pump intensity required to switch the interferometer from the reflecting to transmitting state (or vice versa) can be calculated from the following expression using the known values of n_2 for CS_2 and MBBA.

$$T = \frac{1}{1 + F \sin^2(\delta_o + \nu I_{\text{pump}})}$$

where

$$\delta_o = \frac{2\pi n_o \ell}{\lambda_s}$$

$$\nu = \frac{2\pi n_2 \ell}{\lambda_s} \left(\frac{8\pi}{n_o c} \times 10^{13} \right) \frac{\text{cm}^2}{\text{MW}}$$

$$I_{\text{pump}} = \text{pump intensity (MW/cm}^2\text{)} .$$

Assume that the interferometer is tuned for an initial transmission of $T = 0.25$ ($R = 0.75$) and we wish to switch to $T = 0.75$ ($R = 0.25$), assuming a mirror reflectivity of $R_m = 0.80$ (thus, the finesse $F = 14$). The required pump intensity is given by

$$\nu I_{\text{pump}} = \arcsin(3/F)^{1/2} - \arcsin(.33/F)^{1/2}$$

$$I_{\text{pump}} = .04\pi/\nu$$

$$= \frac{.04\lambda n_o c}{16\pi n_2 l} \times 10^{-13} \text{ MW/cm}^2.$$

The pump intensities required for switching a nonlinear etalon with CS_2 or MBBA as the intracavity medium, along with the n_2 values of CS_2 and MBBA, are given in Table 2.

TABLE 2		
material	$n_2(\text{cm}^3/\text{erg})$	$I_{\text{pump}}(\text{MW/cm}^2)$
CS_2	1.2×10^{-11}	20.1
MBBA	9.0×10^{-11}	2.7

Comparison of Tables 1 and 2 shows that for the same nonlinear material, the nonlinear Fabry-Perot interferometer makes a much more efficient switch than the Kerr effect. This can be attributed directly

to the increased pathlength through the intracavity medium for the signal beam due to the multipass nature of the resonant interferometer. Although the finesse of a Fabry-Perot interferometer is defined as the ratio of the frequency spacing of the transmission maxima to the frequency bandwidth of a single transmission peak, it is also a fairly direct measure of the number of round trip passes the signal beam makes through the resonator. Thus, we see that for an etalon finesse of 14, the switching intensities required in the Kerr effect switch are about 17X greater than those required for the interferometer switch.

We have investigated this type of interferometer switch experimentally using a HeNe signal beam ($\lambda_s = 632.8 \text{ nm}$) and a SHG of Nd:YAG pump beam ($\lambda_p = 532.0 \text{ nm}$) with both CS_2 and allo-ocimene (see next section) as the nonlinear intracavity media. The interferometer mirror reflectivity was $R_m = 0.93$, the mirror spacing was set to 1.6 cm, and an uncoated optical cell (optical pathlength of 8 mm) containing the nonlinear medium was placed in the cavity, canted slightly off axis so that reflections from the cell surfaces would not interfere with the main signal beam. With either liquid in the cell, the measured peak transmission of the interferometer was about 20% and the finesse was measured to be ~ 20 (theoretical finesse for $R_m = .93$ and perfect alignment is $F = 43$). The interferometer was initially tuned to resonance (by piezoelectrically varying the cavity spacing), so that the pump pulse should have caused a decrease in transmission. We were unable to observe this predicted behavior, however, and attribute our difficulty to thermal gradients induced in the nonlinear

liquids by the pump radiation. Thermal gradients cause index gradients that distort the phase front of the signal beam in the cavity, thereby degrading the interferometer's finesse and reducing the transmission of the signal even when the cavity is tuned to resonance. In CS_2 , phase distortion occurred for pump intensities larger than 5 MW/cm^2 , well below the calculated intensity ($\sim 30 \text{ MW/cm}^2$) required to switch the etalon from the transmitting to reflecting state; the behavior of the allocimene was comparable. In both cases, the interferometer finesse and transmission recovered after the pump radiation was turned off with a time constant of one or two seconds.

IV. THIRD-ORDER NONLINEAR SUSCEPTIBILITY

A. $\chi^{(3)}$ in Liquids and Solids

The two types of switches outlined in the preceding sections would both be feasible if materials with larger values of $\chi^{(3)}$ were available. Unfortunately, CS_2 seems to have the largest $\chi^{(3)}$ of any liquid reported in the literature,⁸⁻¹² with the exception of some of the liquid crystals,⁴ whose importance to this application can be discounted because of their slow response and requirement of being kept at a constant, elevated temperature.

In an effort to find liquids with larger nonlinear susceptibilities, we have examined solutions of several linear conjugated molecules, a class of organic molecules that has been reported^{13,14} to show very large values of $\chi^{(3)}$. The polarizability of the molecules in this class increases nonlinearly with the length of the molecule due to the π electron delocalization associated with the conjugated double bonds, resulting in strong enhancement of the electronic contribution to nonlinear optical properties with increasing chain length. We have measured the relative magnitude of the optical Kerr coefficient B for several conjugated molecules with respect to that of CS_2 using the experimental arrangement shown in Fig. 3, with $\lambda_p = 1.06 \mu$ (Nd:glass laser) and $\lambda_s = 632.8 \text{ nm}$ (HeNe laser). The results are given in Table 3. Only allo-ocimene has a B value that is somewhat larger than that of CS_2 . This does not conflict with Hermann's report¹⁴ of increasing nonlinearity with chain length but merely reflects the fact that the saturation concentration of the molecules in a solvent decreases with increasing chain length, partially offsetting the concomitant increase in nonlinearity due to the reorienta-

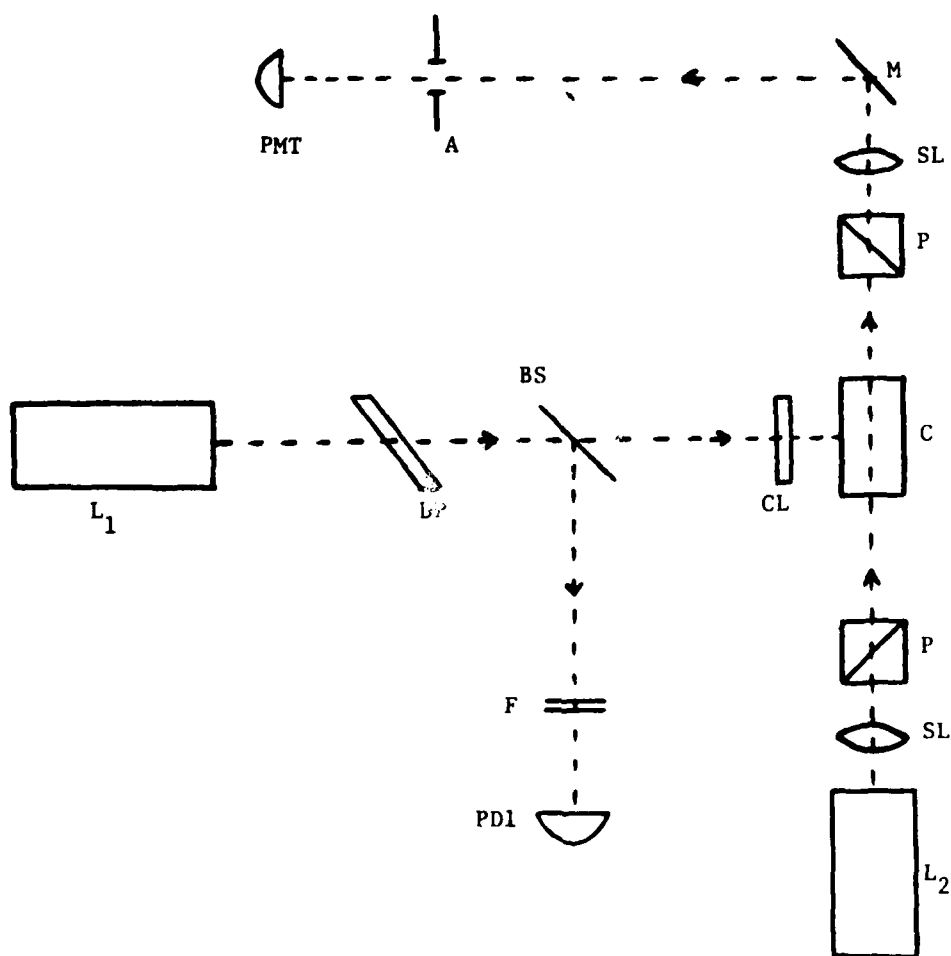


FIGURE 3. Experimental arrangement for measuring relative magnitude of $\chi^{(3)}$ in conjugated molecules. The code is: L_1 , Q-switched Nd:glass laser (1.06μ); L_2 , HeNe laser ($.633 \mu$); DP, dielectric polarizer at 1.06μ ; BS, uncoated glass beamsplitter; F, filters; PD1, photodiode detector to monitor 1.06μ radiation; CL, cylindrical lens; SL, spherical lenses; P, calcite polarizers; C, cell containing nonlinear liquid; M, mirror; A, aperture; PMT, S-20 photomultiplier detector.

tional and electronic contributions per molecule. Thus, the overall nonlinear susceptibility of a pure liquid, like allo-ocimene ($N = 3.6 \times 10^{21}$ molecules/cm³) with few double bonds (3), is larger than that of a much longer molecule like β -carotene ($N \approx 10^{19}$ molecules/cm³ in benzene¹³). Our conclusion is that CS₂ and allo-ocimene have the largest optical nonlinearities of any liquids available to us for practical device applications, and they are comparable.

Thus far we have considered only liquids as nonlinear media for switch applications, primarily because the molecular densities of gases are much too low to yield large macroscopic values of $\chi^{(3)}$, and the use of solids introduces several new problems, the most serious of which are their low thresholds for optical damage and their poor optical quality. The most highly nonlinear class of solids, with the fastest change in the refractive index (all electronic), seems to be the semiconductors, many of which are relatively soft and therefore difficult to polish. The resulting small surface scratches and imperfections reduce even further their threshold for laser intensity induced surface damage. A further problem with solid media is that they often exhibit bulk strain induced birefringence which can allow an undesirable amount of the signal beam to leak through the analyzer in the Kerr effect switch, thus decreasing its dynamic range. The Fabry-Perot interferometer type of switch requires homogeneous intracavity media with flat surfaces for optimum performance, since phase distortions in the wave front of the signal beam can severely degrade the finesse of the interferometer (e.g., surfaces polished flat

TABLE 3			
Conjugated Molecule	No. of Double Bonds	Solvent	$\chi^{(3)} / \chi^{(3)}_{CS_2}$
Isoprene	2	pure liquid	$0.1 \pm 10\%$
Allo-ocimene	3	pure liquid	$1.7 \pm 10\%$
all-trans Retinol	5	chloroform	$0.1 \pm 10\%$
all-trans Retinal	6	chloroform	$0.4 \pm 10\%$
β -Carotene	11	benzene	$0.4 \pm 10\%^*$

* This value includes a contribution from the nonlinear susceptibility of benzene ($\chi_{benzene} / \chi_{CS_2} = .14^{11}$).

TABLE 4		
Material	Wavelength (μm)	$\chi^{(3)}$ (cm^3/erg)
CS_2 (liquid)	.6943	3.1×10^{-12}
Ge (m3m)	10.6	$1.0 \quad 50\% \times 10^{-10}^*$
Si (m3m)	10.6	$6. \quad 50\% \times 10^{-12}^*$
GaAs ($\bar{4}3m$)	10.6	$9.7 \times 10^{-12} \quad 16^{**}$
CuC ($\bar{4}3m$)	.6943	$3.3 \quad 2.0 \times 10^{-12}^{***}$

* Ref. 15

** Ref. 16

*** Ref. 17

to $\lambda/20$ over the signal beam aperture will limit the cavity finesse to 10), thus decreasing the switch's sensitivity to the induced index change and lowering the maximum resonant transmission. The $\chi^{(3)}$ values of only a few semiconductors have been reported, and they are given in Table 4, along with the corresponding value for CS_2 used as a reference. As can be seen, with the exception of Ge (which is opaque for wavelengths shorter than 1.9μ), semiconductors offer no significant increase in $\chi^{(3)}$ over the liquids considered thus far, so in light of the other difficulties associated with solids, we can conclude that they are not practical media for use in the nonlinear switches described previously.

B. Resonant Enhancement of $\chi^{(3)}$

So far in this report, we have treated the nonlinear susceptibility of each material as a dispersionless constant, independent of ω_p , ω_s , or any combination of ω_p and ω_s . This is only approximately correct, for although $\chi^{(3)}$ is fairly constant over broad ranges of frequency, it can experience strong resonant enhancements for certain values of ω_p , ω_s , and $\omega_p \pm \omega_s$. Therefore, $\chi^{(3)}$ is usually written as the sum of a nonresonant term ($\chi_{NR}^{(3)}$) and of several resonant terms ($\chi_{RES}^{(3)}$) which individually may become important only for specific input frequencies and combinations of input frequencies.

$$\chi^{(3)} = \chi_{NR}^{(3)} + \sum \chi_{RES}^{(3)} \quad (1)$$

All nonlinear coefficients reported so far were based solely on the nonresonant susceptibility $\chi_{NR}^{(3)}$ due to electronic and reorientational contributions. The resonant term in Eq. (1) is summed over several types of resonances, which include, in two frequency experiments, one-photon resonances (ω_p , ω_s), two-photon resonances ($2\omega_p$, $2\omega_s$, $\omega_p + \omega_s$), and Raman resonances ($\omega_p - \omega_s$). The requirement for a resonant enhancement to occur is that there be a real transition in the nonlinear medium corresponding to the exciting incident frequency or to an appropriate sum or difference of incident frequencies. For two beam experiments of the type discussed in the first two sections, the most important resonances are the Raman type, i.e., internal vibrational contributions to $\chi^{(3)}$, which occur when the difference between input frequencies ($\omega_p - \omega_s$) is equal to a vibrational frequency (phonon) characteristic of the nonlinear liquid

(solid).¹⁸

In the vicinity of an isolated Raman resonance, the dominant term in the sum over $\chi_{\text{RES}}^{(3)}$ in Eq. (1) is

$$\chi_{\text{RAMAN}}^{(3)} = \frac{N(\alpha_{||})^2/48hc}{\omega_R - (\omega_p - \omega_s) + i\Gamma_R} \quad (2)$$

where N = molecular density of medium

$(\alpha_{||})^2$ = diagonal Raman tensor element per molecule

ω_R = frequency of the Raman vibration

Γ_R = linewidth (HWHM) of the Raman vibration.

This resonant susceptibility is proportional to the differential spontaneous Raman scattering cross section per molecule ($d\sigma/d\Omega$) for the mode at ω_R through the relationship

$$(\alpha_{||})^2 = \left(\frac{c}{\omega_s}\right)^4 \left(\frac{d\sigma}{d\Omega}\right)$$

From Eq. (2) we see that the amount of the enhancement in $\chi^{(3)}$ when $(\omega_p - \omega_s)$ is tuned exactly to ω_R is determined by Γ and $d\sigma/d\Omega$. The inverse dependence on Γ is a common feature of $\chi_{\text{RES}}^{(3)}$ due to non-Raman mechanisms as well and results in only modest enhancements when one- or two-photons are resonant with a broad absorption band.

For both the Kerr switch and the Fabry-Perot interferometer switch, the signal at the detector depends upon the square of the induced phase

change experienced upon traversing the medium, and therefore on the square of the magnitude of $\chi^{(3)}$. Thus,

$$I_s \propto |\chi_{NR}^{(3)} + \chi_{RAMAN}^{(3)}|^2$$

$$\propto \frac{[\omega_R - \Delta\omega + \Lambda\Gamma]^2 + \Gamma^2}{[\omega_R - \Delta\omega]^2 + \Gamma^2}, \quad (3)$$

where $\Delta\omega = \omega_p - \omega_s$, and we have defined a resonant enhancement parameter, Λ , where

$$\Lambda \equiv \frac{N(\alpha_{||})^2}{48hc\Gamma\chi_{NR}^{(3)}}.$$

Equation (3) is plotted in Fig. 4 as a function of the frequency difference $\Delta\omega$ tuned through ω_R , assuming an enhancement factor $\Lambda = 2.0$ and linewidth $\Gamma = 1.0 \text{ cm}^{-1}$. Note that the peak intensity depends solely on Λ ; thus Λ is an indicator of the amount of enhancement in $\chi^{(3)}$ obtained by tuning to a Raman resonance. Values of Λ for several liquids have been reported in a recent publication¹⁹ and are listed in Table 5 along with their corresponding values of $\chi_{NR}^{(3)}$. Only C_6H_{12} exhibits significant resonant enhancement, but its $\chi_{NR}^{(3)}$ is so small that its overall $\chi^{(3)}$ on Raman resonance is still much smaller than $\chi_{NR}^{(3)}$ for CS_2 .

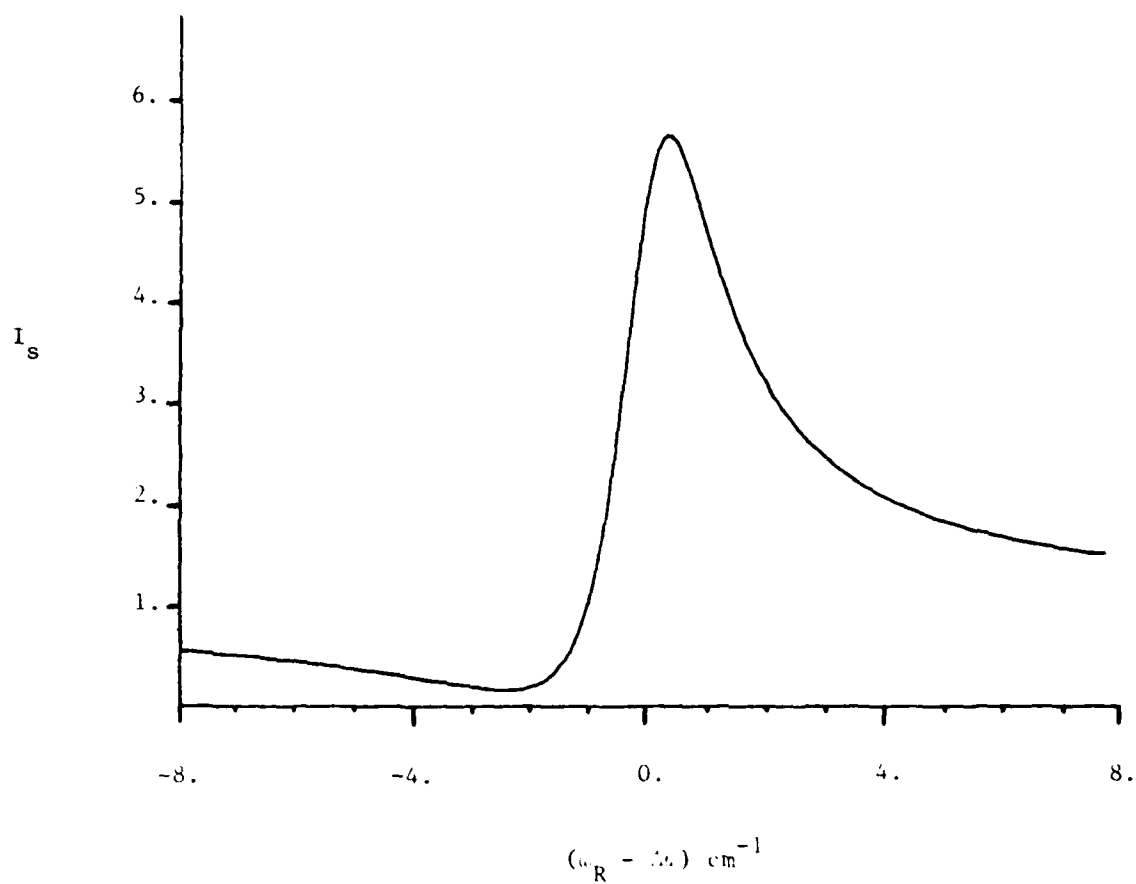


FIGURE 4. Plot of Eq. (3). Vertical axis is proportional to the signal intensity (I_s); horizontal axis is the mistuning of the difference between the signal and pump frequencies ($\omega_p - \omega_s$) from the Raman mode (ω_R). Values of the parameters in Eq. (3) are $\Lambda = 2.0$, $\Gamma = 1.0 \text{ cm}^{-1}$.

TABLE 5			
<u>Liquid</u>	<u>ω_R (cm⁻¹)</u>	<u>Λ</u>	<u>$\chi_{NR}^{(3)}$ (10⁻¹⁴ cm³/cig)</u>
C ₆ H ₆	992	1.88 ± 0.08	4.23 ± 0.19
CS ₂	656	1.02 ± 0.11	23.4 ± 1.2
C ₆ H ₅ Cl	1002	0.73 ± 0.05	7.62 ± 0.53
C ₆ H ₅ N	991	1.07 ± 0.07	4.46 ± 0.3
C ₆ H ₁₂	802	4.15 ± 0.25	0.56 ± 0.04

V. FABRY-PEROT INTERFEROMETER SWITCH - NONLINEAR ABSORPTION

Because of its multipass nature, a resonant Fabry-Perot interferometer is sensitive not only to induced index changes in the intracavity medium but to induced absorption as well, so that a small change in absorption within the cavity can have a large effect on the total transmission and reflection of the etalon. In the following section, we will show that it is possible to make an effective light activated switch by placing a material whose absorption at ω_s increases with the light intensity at ω_p (nonlinear absorber) within the interferometer cavity.

The transmission (T) and reflectivity (R) of a Fabry-Perot interferometer with an absorbing intracavity medium are (in the plane wave approximation, assuming perfectly flat and parallel mirrors)

$$T = \frac{(1 - R_m)^2 e^{-\alpha l} / (1 - R_m e^{-\alpha l})^2}{1 + F \sin^2(kl)}$$

$$R = \frac{R_m \left(\frac{1 - e^{-\alpha l}}{1 - R_m e^{-\alpha l}} \right)^2 + F \sin^2(kl)}{1 + F \sin^2(kl)},$$

where

$$F = \frac{4R_m e^{-\alpha l}}{(1 - R_m e^{-\alpha l})^2}$$

α = absorption coefficient of intracavity medium.

With the cavity tuned to resonance [$\sin(kl) = 0$], these expressions reduce to

$$T = \frac{(1 - R_m)^2 e^{-\alpha l}}{(1 - R_m e^{-\alpha l})^2} \quad (4)$$

$$R = R_m \left(\frac{1 - e^{-\alpha l}}{1 - R_m e^{-\alpha l}} \right)^2 \quad (5)$$

Note that if α is set equal to zero, these expressions yield $T = 1$, and $R = 0$; and if $\alpha \gg l^{-1}$, they yield $T = 0$, and $R = R_m$. The latter result is to be expected, since an opaque intracavity medium will prevent the signal beam from reaching the second mirror of the interferometer, in which case the problem reduces to simple reflection from a single mirror of reflectivity R_m . In Fig. 5 we have plotted T and R from Eqs. (4) and (5) as functions of the absorption α for five values of finesse, assuming $l = 1.0$ cm. The $F = 0$ curves correspond to the case of single-pass absorption of ω_s , i.e., no cavity is present. These curves show that the use of a cavity of even modest finesse (~ 10) dramatically enhances the sensitivity to α over the single-pass case.

The behavior of a switch based on this device can be deduced from Fig. 5. The cavity is initially tuned to resonance at ω_s so the transmission of the signal is high and the reflectivity is low. When the strong beam at ω_p is present, the induced absorption at ω_s will destroy the finesse of the cavity, thus causing the signal to be reflected rather than transmitted. In a high finesse cavity, a relatively small increase in α will result in a large decrease in T with little energy loss in the absorbing medium (in the limiting case, the loss $= 1 - R_m$). The advantages of

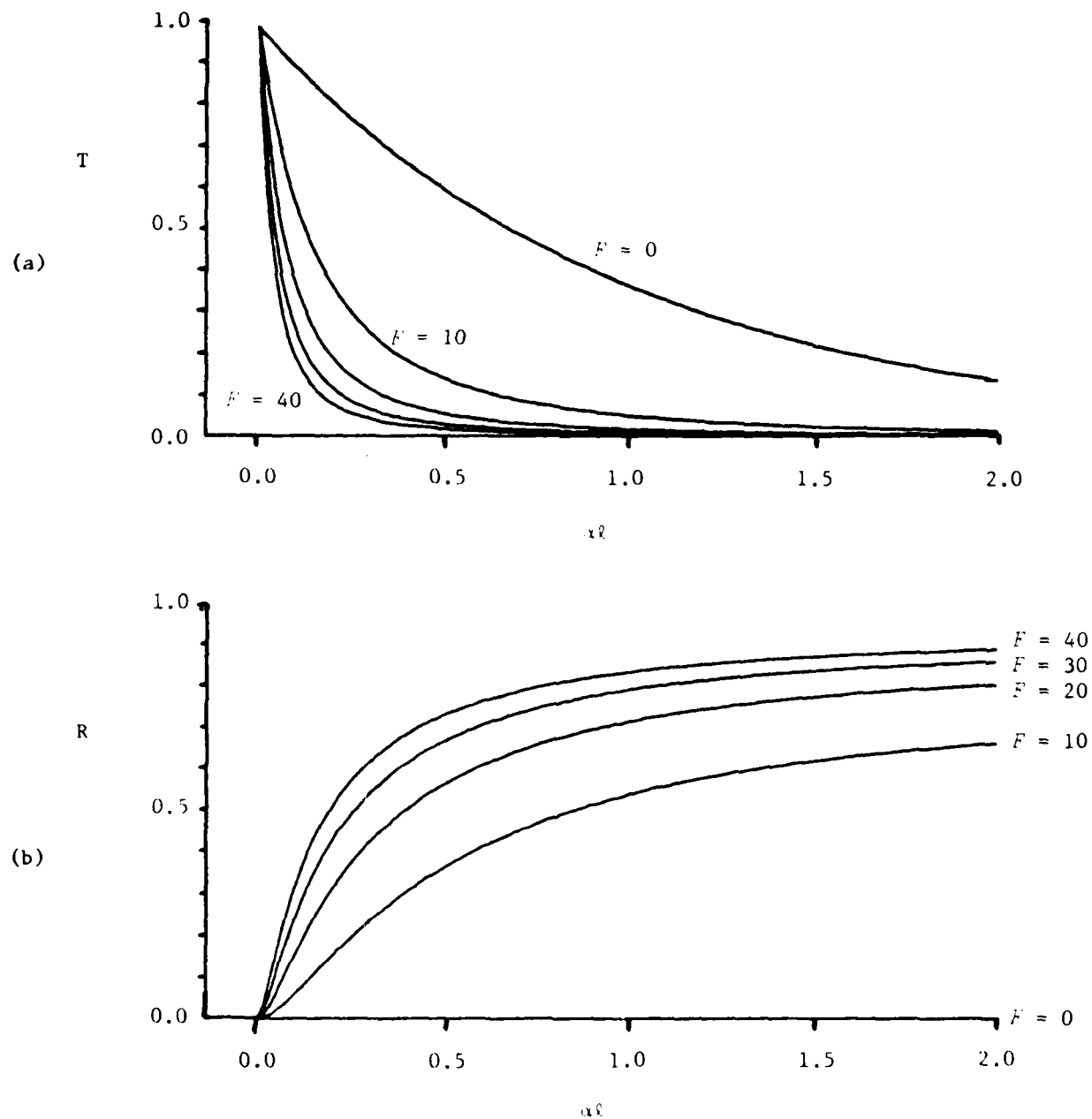


FIGURE 5. (a) Transmission of a resonant Fabry-Perot interferometer as a function of the intracavity absorption, α , for different values of finesse ($F = 0, 10, 20, 30, 40$) [Eq. (4)]. (b) Reflectivity of the resonant interferometer for the same conditions as in (a) [Eq. (5)].

placing the absorber in a resonant cavity are two-fold: (1) the switch sensitivity to induced absorption is increased over the single-pass case; and (2) much of the signal that is not transmitted is reflected by the etalon, rather than simply lost to absorption, as occurs in the single-pass case.

In general, one will expect to introduce some linear loss at frequency ω_s by inserting a liquid or solid medium in the interferometer cavity, either due to surface reflections, scattering or linear absorption. If all of these losses are described by a single, effective absorption coefficient α_o , we can write the total absorption coefficient as

$$\alpha = \alpha_o + \alpha_1(I_p)$$

where $\alpha_1(I_p)$ is written to show that the induced absorption depends upon the pump beam intensity. With an initial absorption α_o and mirror reflectivity R_m , one finds that the finesse is

$$F = \frac{\pi\sqrt{R_m}e^{-\alpha_o l}}{(1 - R_me^{-\alpha_o l})} \quad (6)$$

For $\alpha_o = 0$, this reduces to the usual form $F = \pi\sqrt{R_m}/(1 - R_m)$. We see that the effect of α_o is to decrease the finesse [Eq. (6)], which decreases the peak transmission [Eq. (4), Fig. 5] and increases the reflectivity of the interferometer. For a given value of α_o , then, it is important to choose R_m carefully so that the initial transmission of the etalon is

sufficiently high, but the finesse is not too severely degraded. For example, if $\alpha_0 \ell = .05$ and $R_m = 0.90$, the finesse = 20.2 and $T = .46$, so that although the finesse is high, the maximum transmission of the switch is only 46% in the 'on' state, and the reflected component is 0.10 (ideally $R = 0$). A better choice of mirror reflectivity would be $R_m = .65$, which would result in a low finesse ($F = 6.5$), but good transmission in the 'on' state ($T = .80$, $R = .08$). In Fig. 6 we have plotted T , R , and $1 - (T + R)$ (loss to absorption) for an etalon with $\alpha_0 \ell = .02$ (which corresponds to a single-pass loss through medium of 2.0%) and $R_m = .85$. For these values, the interferometer has a finesse of 17.2. In the 'on' state ($\alpha = \alpha_0$), the transmission is 79.2% and $R = 1.2\%$. In the 'off' state (in which we assume $\alpha = 1.0 \text{ cm}^{-1}$), the reflectivity is 71.9% and $T = 1.8\%$. Thus, the net loss of the switch is $\sim 30\%$.

We have investigated this type of switch with media that owe their nonlinear absorption properties to two different mechanisms: (1) excited-state absorption, and (2) two-photon absorption. In an excited-state absorber, the ω_p beam is partially or fully absorbed in the medium, thus exciting part of the ground state population into the absorbing state. The beam at ω_s , which initially traversed the sample (in its ground state) without any absorption, then excites transitions from the excited state (populated by ω_p) to even higher lying levels. The sample thus absorbs radiation at ω_s until the excited state population decays away (with time constant τ). This dependence of the absorption at ω_s upon a material parameter (τ) rather than upon the pump pulse duration is a disadvantage

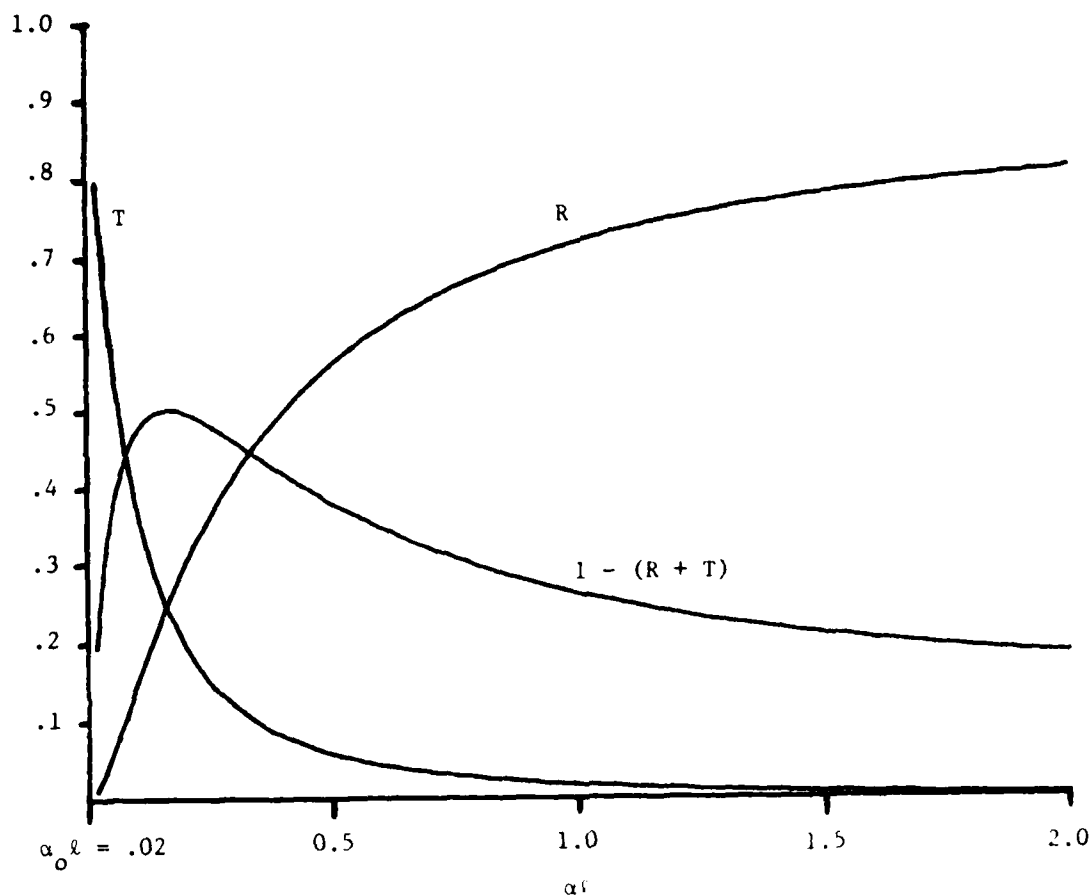


FIGURE 6. Transmission (T), reflectivity (R), and absorptive loss $[1 - (R + T)]$ of a resonant Fabry-Perot interferometer as a function of the intracavity absorption. The initial cavity characteristics are: $\alpha_0 \ell = .02$ and $R_m = .85$, yielding a finesse of 17.

for fast switching applications because many relatively efficient excited state absorbers have long excited state lifetimes and would thus limit the duty cycle of the switch.

Two-photon absorption is a nonlinear optical [$\chi^{(3)}$] effect in which photons from each of the two input beams (ω_s, ω_p) are simultaneously absorbed, although neither photon individually is energetic enough to excite any transitions in the medium (i.e., the medium is transparent to ω_p and ω_s). The transmission of the signal beam is described by

$$I_s(z) = I_s(0)e^{-\beta I_p z}$$

where β = two-photon absorption coefficient (frequently expressed in units of cm/MW and I_p is the pump beam intensity (MW/cm^2). Because there are no intermediate states to be populated, the duration of the absorption at ω_s is determined by the pump beam duration, not by any material parameters. Thus, unlike the case with many excited-state absorbers, it is possible to induce nanosecond duration absorption at ω_s . The disadvantage of two-photon absorption is that it is usually a weaker effect than excited state absorption.

A. Intracavity Excited-State Absorber

Our first experiments on the nonlinearly absorbing Fabry-Perot interferometer switch were done with glasses exhibiting strong excited-state absorption as the nonlinear media. Glass media are attractive for this application because they can be made with good optical quality and are relatively hard, thus making it possible to cut and polish them to the flatness required for intracavity use. We therefore searched through 30 glass color filters from Schott, Hoya and Corning in an effort to find the sample with the largest absorption at 632.8 nm induced by a 10 ns duration pump pulse at 532.0 nm (these laser wavelengths were chosen because they were conveniently available in our lab). We found that the best choice was Schott OG-530, an orange, sharp-cut, long wavelength pass filter with its absorption edge near 532.0 nm ($\alpha_{532.0} = 1.5 \text{ cm}^{-1}$). The characteristics of this material were measured using the experimental set-up shown in Fig. 7, and the results are shown in Fig. 8. Figure 8(a) shows the transmission through a 3 mm thick sample as a function of the pump energy density (1.0 J/cm^2 corresponds to a 2.5 mJ pulse). Figure 8(b) is a photograph of an oscilloscope trace showing the time decay of the induced absorption of the signal beam. The relaxation time of the tail is estimated to be $\sim 40 \text{ } \mu\text{s}$. Although the optical quality of Schott filter glass is not very good, we were able to obtain a special piece from Schott with very low inhomogeneity ($\Delta n \leq 2 \times 10^{-6}$) and had it polished with two opposite faces flat to $\lambda/20$. The measured transmission at Brewster's angle was only about 88% at ω_s , which implies an $\alpha_0 = .14 \text{ cm}$ (pathlength through the sample at Brewster's angle is .89 cm). This is much higher

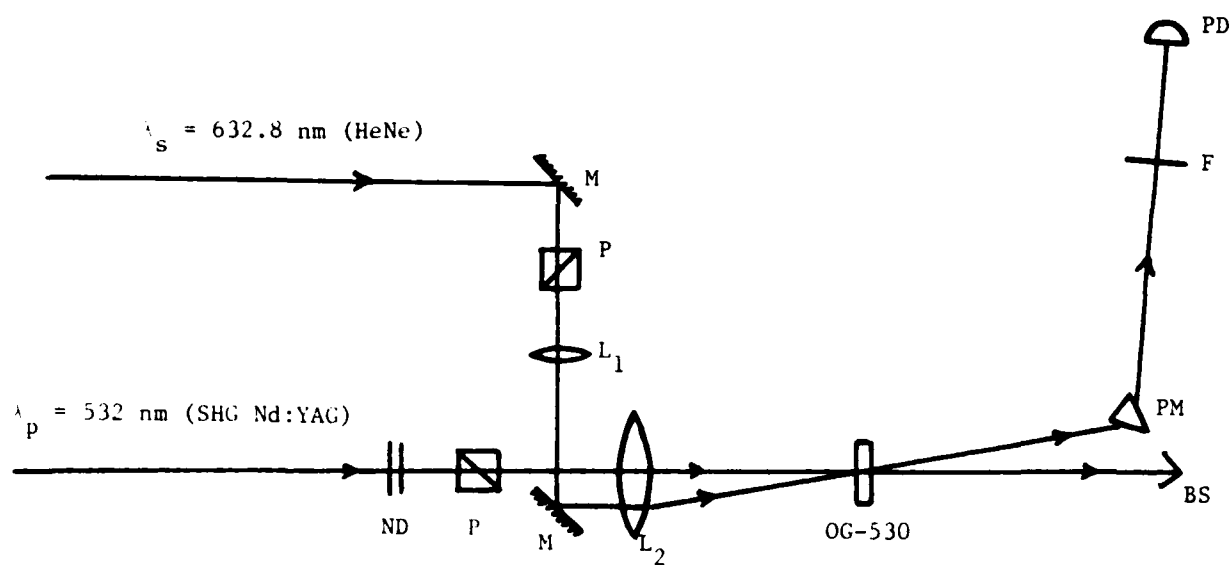
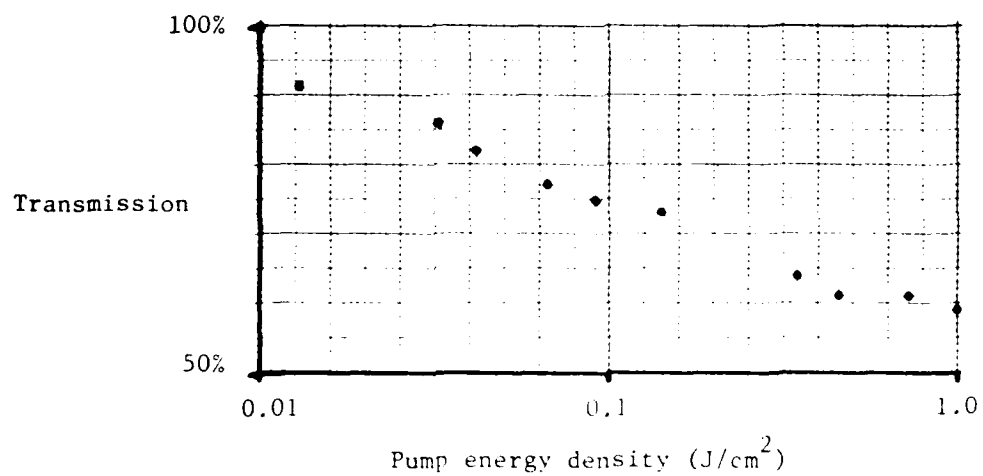


FIGURE 7. Experimental arrangement used to measure excited-state absorption in filter glass OG-530. The code is: P, polarizers; M, mirrors; ND, neutral density filters; L_1 , 50 cm focal length lens; L_2 , 36 cm focal length lens; BS, beam stop; F, 632.8 nm interference filter; PM, prism; PD, photodiode detector. The pump and signal beams cross in the sample at an angle of $\sim 5^\circ$.

FIGURE 8



- (a) Transmission of 3 mm thick OG-350 color filter as a function of the pump energy density, measured with the apparatus shown in Fig. 7.



- (b) Time decay of the excited state absorption in OG-350 glass. Horizontal time axis is 200 nsec/cm.

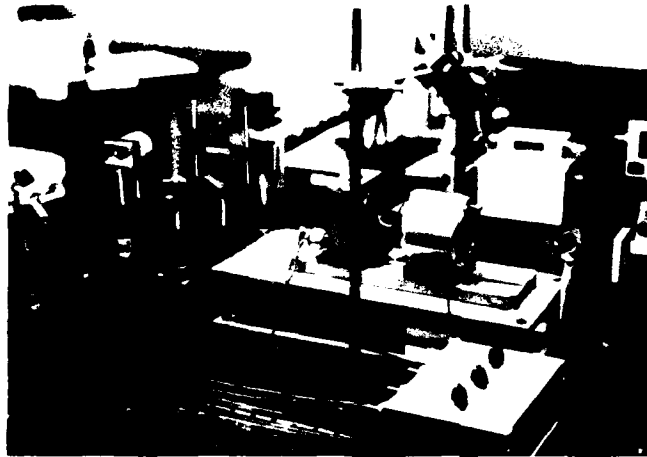
than anticipated from measurements made on the original filter; the difference is probably due to melt-to-melt variations in the glass production.

With this piece placed in the interferometer cavity ($R_m = .93$ at 632.8 nm), we did observe the expected switching behavior with the experimental arrangement shown in Fig. 9. Figure 10 shows the decrease in transmission observed when the sample is within the cavity [Fig. 10(a)], and when the cavity is removed [Fig. 10(b)], for the same pump intensity. In this case, an induced single-pass absorption of 24% caused a decrease of the interferometer transmission to $\sim 24\%$ of its initial value. Thus, the effective 'gain' of the interferometer was about a factor 3. However, the overall transmission of the interferometer was only 14% because of the large linear absorption in the OG-530 glass. The calculated values of the transmission, reflectivity and finesse of a cavity with $\alpha_0 = .14 \text{ cm}^{-1}$, $l = .89 \text{ cm}$, and $R_m = .93$, are given in Table 6 along with the measured values.

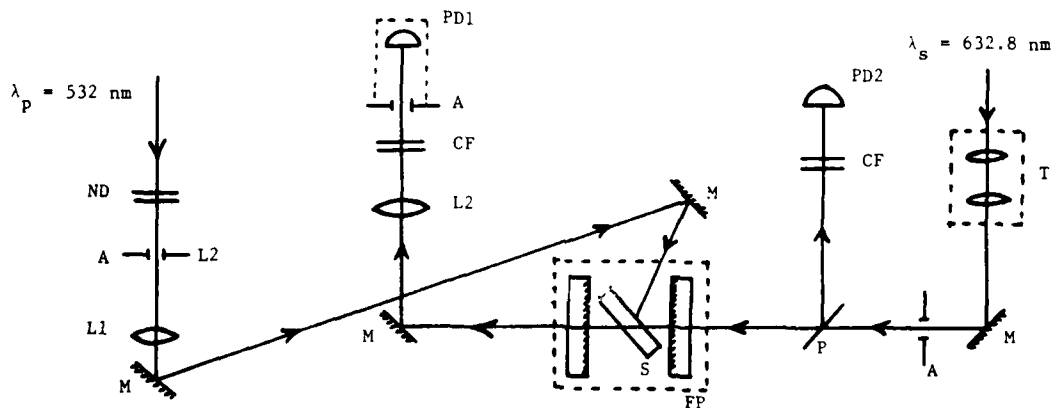
TABLE 6			
	T	R	F
Calculated	.14	.40	16
Measured	.17	.57	14

For a cavity with finesse 14, an induced single-pass absorption of 24% is calculated to yield a transmission of 20%, which is in reasonable agreement with the measured value of 24%.

FIGURE 9

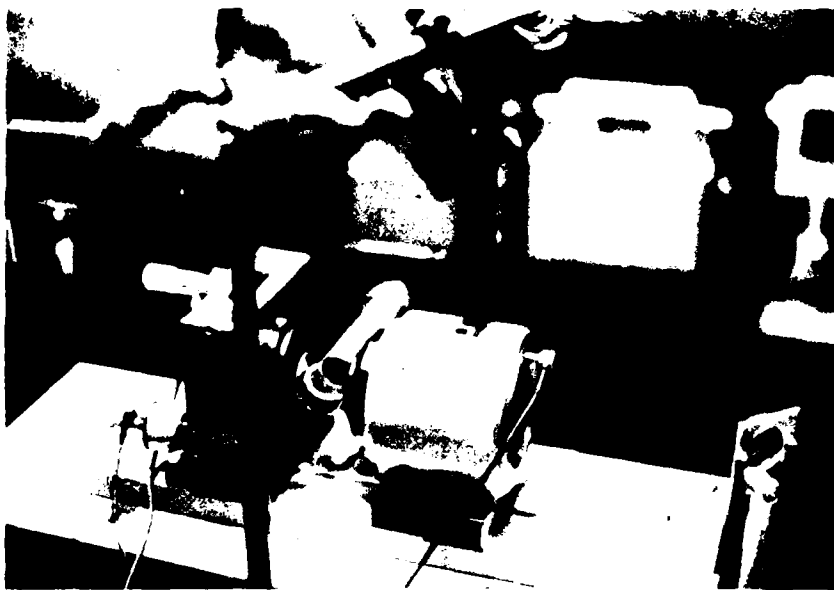


(a) Photograph of experimental set-up used in investigation of the Fabry-Perot interferometer optical switch.



(b) Schematic diagram corresponding to photograph in (a). The code is: M, mirrors; A, apertures; L1, 50 cm focal length lens; L2, 25 cm focal length lens; ND, neutral density filters; CF, color filters to block 532 nm; P, pellicle beamsplitter; FP, Fabry-Perot interferometer; T, telescope; S, intracavity nonlinear absorber; PD1, photodiode monitoring transmitted signal; PD2, photodiode monitoring reflected signal.

FIGURE 9
(Continued)



(c) Close-up view of the interferometer cavity with the CdS crystal in place at Brewster's angle.

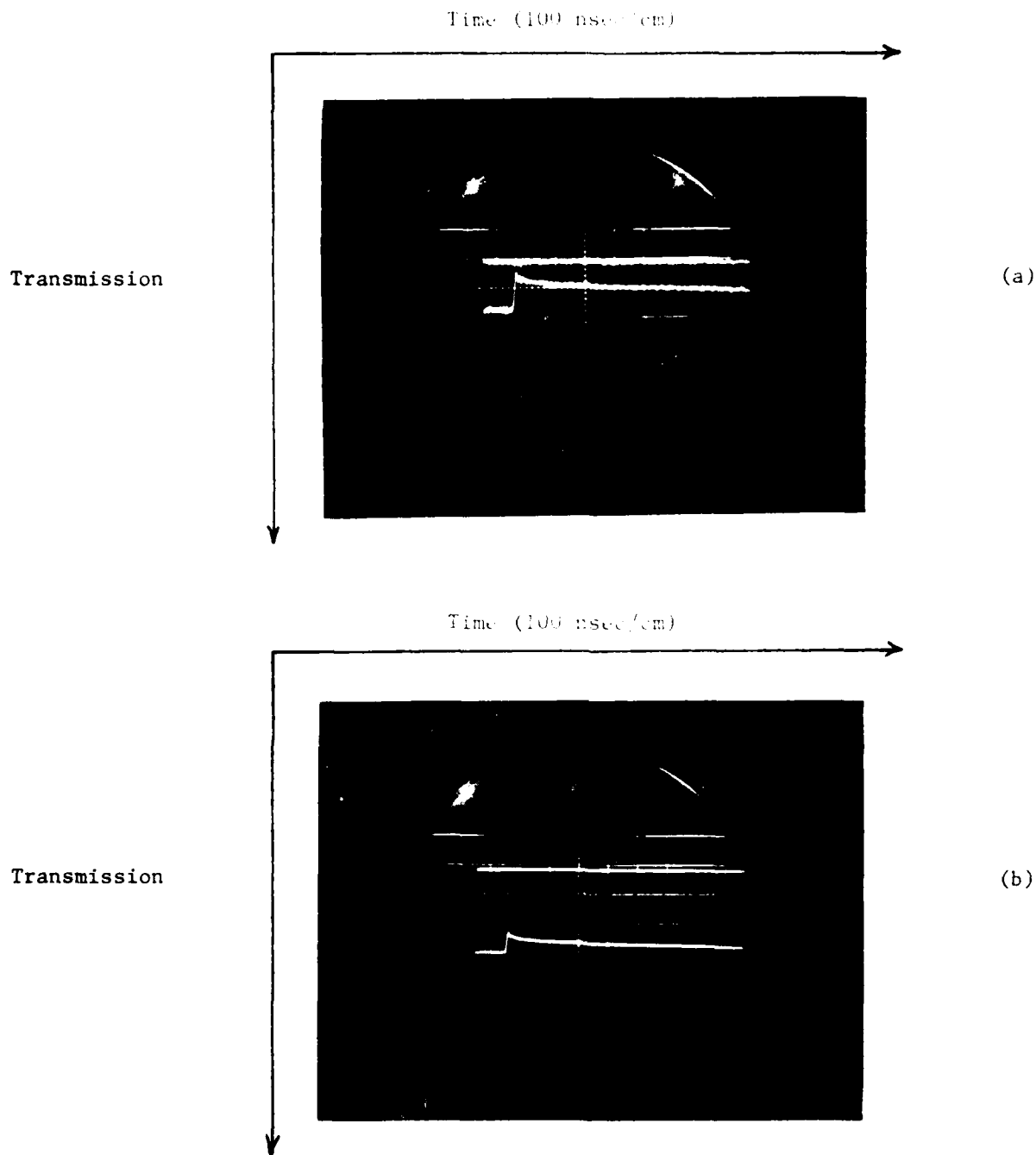


FIGURE 10. Experimental results with OG-530 excited-state absorber ($\alpha_0 = .14 \text{ cm}^{-1}$).

(a) Pump induced decrease in transmission of interferometer with intra-cavity OG-530 glass.

(b) Pump induced decrease in single-pass transmission of OG-530 due to excited-state absorption (measured external to interferometer).

Pump powers in (a) and (b) are identical; in both photographs, the upper trace is the zero transmission level.

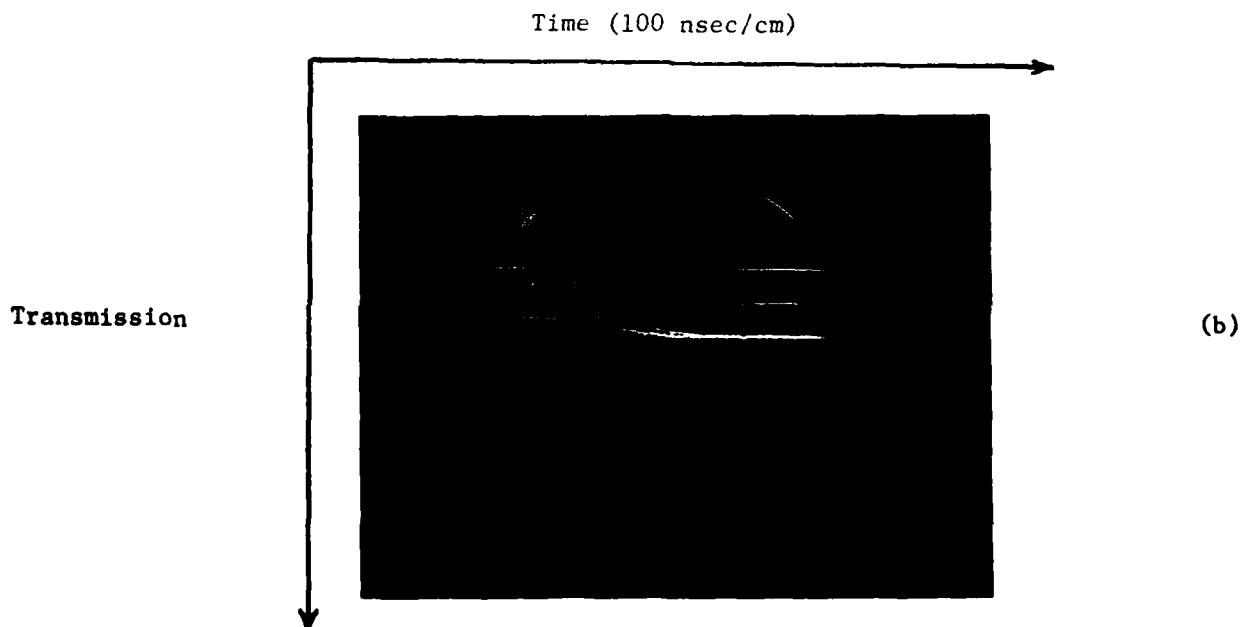
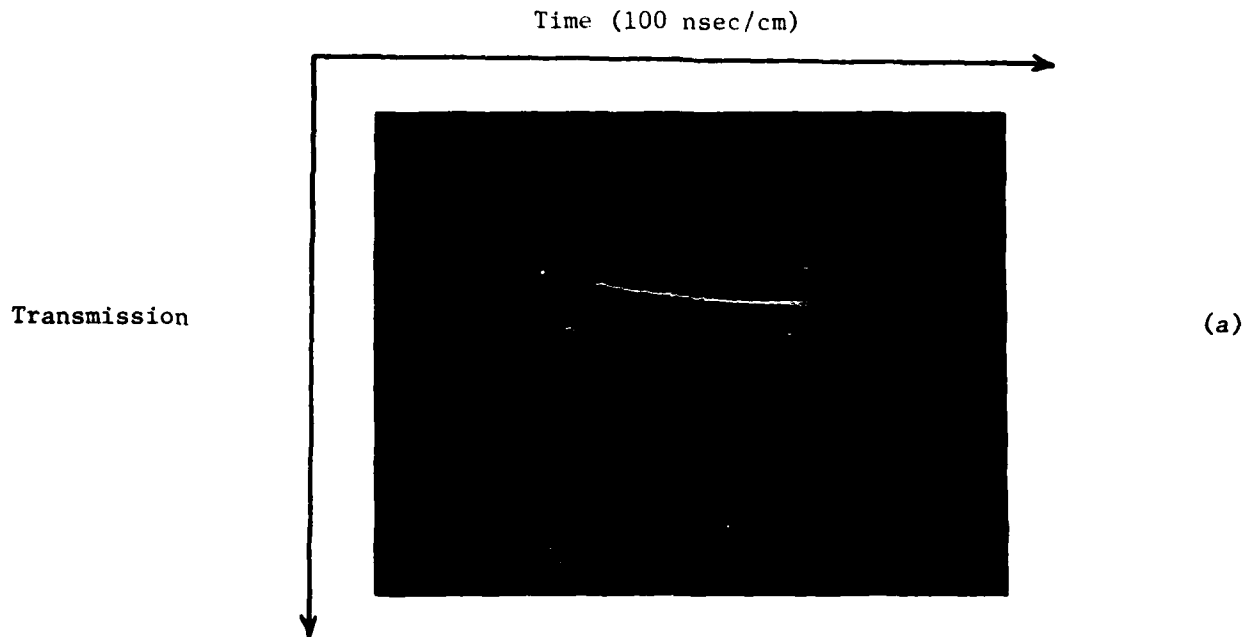
In an effort to improve the transmission of the switch, we replaced the special piece of OG-530 material with an ordinary OG-530 color filter (3 mm thick). At Brewster's angle, the single-pass loss was $< 1\%$, which implies $\alpha_o < .03 \text{ cm}^{-1}$. The measured transmission and finesse of the cavity with and without the filter glass are given in Table 7.

TABLE 7		
	Empty Resonator	OG-530 Filter
T	$70 \pm 10\%$	$50 \pm 10\%$
F	30	14

For $R_m = .93$ and $\alpha_o = .03 \text{ cm}^{-1}$, we calculate $F = 36$; the low value of the measured finesse is probably due to bulk inhomogeneities and nonflat surfaces of the filter. The measured finesse of the empty cavity is also well below the calculated finesse ($F = 43$), probably due to surface error in the cavity mirrors (mirror surfaces are flat to $\lambda/20$ over the entire aperture; over the 1 to 2 mm diameter region probed by the HeNe laser, the flatness should be better, but probably is not good enough to allow a finesse of 43).

Figure 11 shows the induced change in transmission with the filter glass in the cavity. In Fig. 11(a) and (b), the switch is initially in the transmitting state and is switched to $T \sim 15\%$ by a pump beam with energy density of $.02 \text{ J/cm}^2$ (single pass $T \approx 93\%$). The only difference between

FIGURE 11



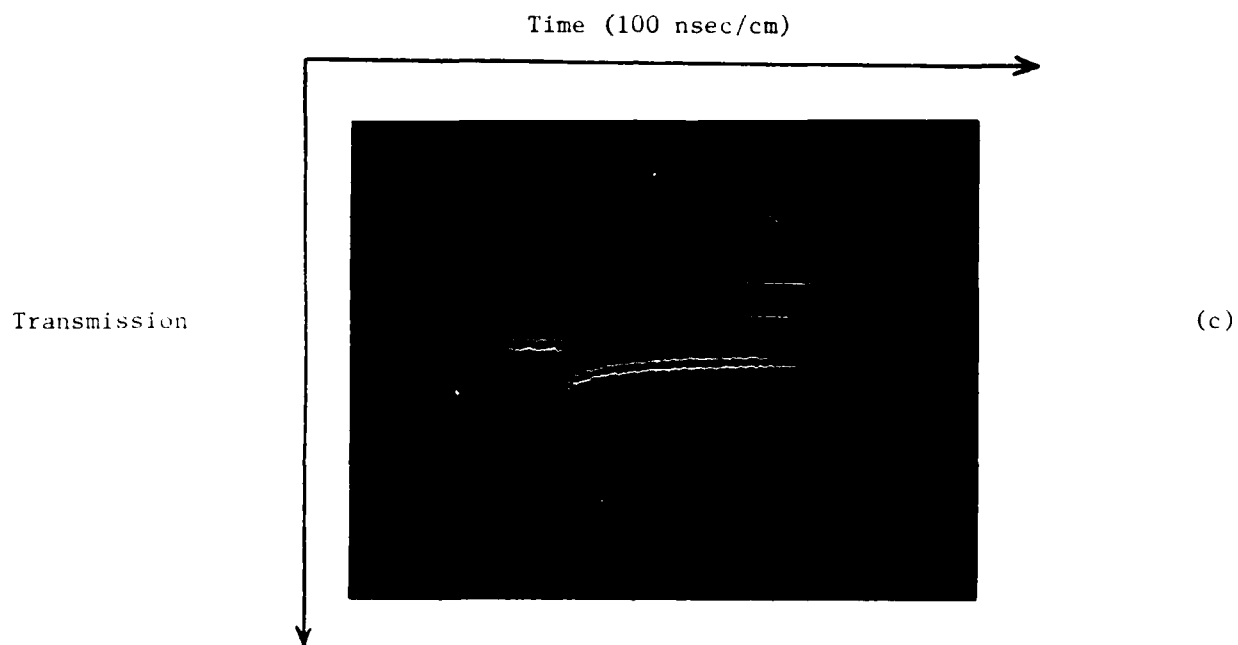


FIGURE 11. Pump induced change in transmission of Fabry-Perot interferometer with intracavity OG-530 color filter. (a) and (b) differ only in the initial tuning of the cavity. (c) shows pump induced increase in transmission for different initial tuning and lower pump energy than in (a) or (b).

the conditions for (a) and (b) is the initial tuning of the cavity. In Fig. 11(c), the etalon is initially partially transmitting, and the transmission is increased by a pump beam with energy density $.007 \text{ J/cm}^2$. The behavior indicated by these three photographs is completely different from that observed with the other OG-530 sample. In this case, the induced change in transmission is due to an induced change in refractive index, rather than to induced absorption. It is not possible for an increase in absorption to cause an increase in transmission of the interferometer. In addition, the induced absorption measured for the conditions in Fig. 11 is too small to account for the large observed changes in etalon transmission. For the conditions of Fig. 11(a), the single-pass absorption was measured to be 7%, which would result in an interferometer transmission of 60% (cavity finesse = 15). This is greater than the observed value of 15%. We attribute this behavior to an index change in the sample induced by the partially absorbed pump beam and will discuss possible mechanisms for this effect later on in the report.

B. Intracavity Two-Photon Absorber

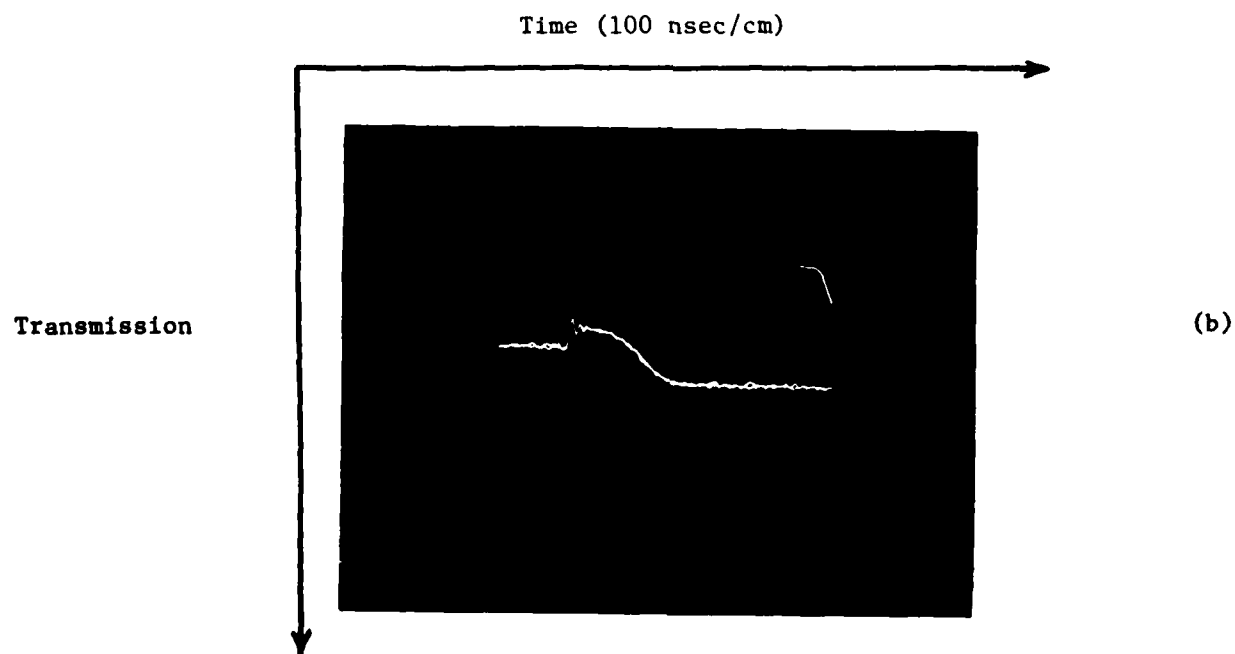
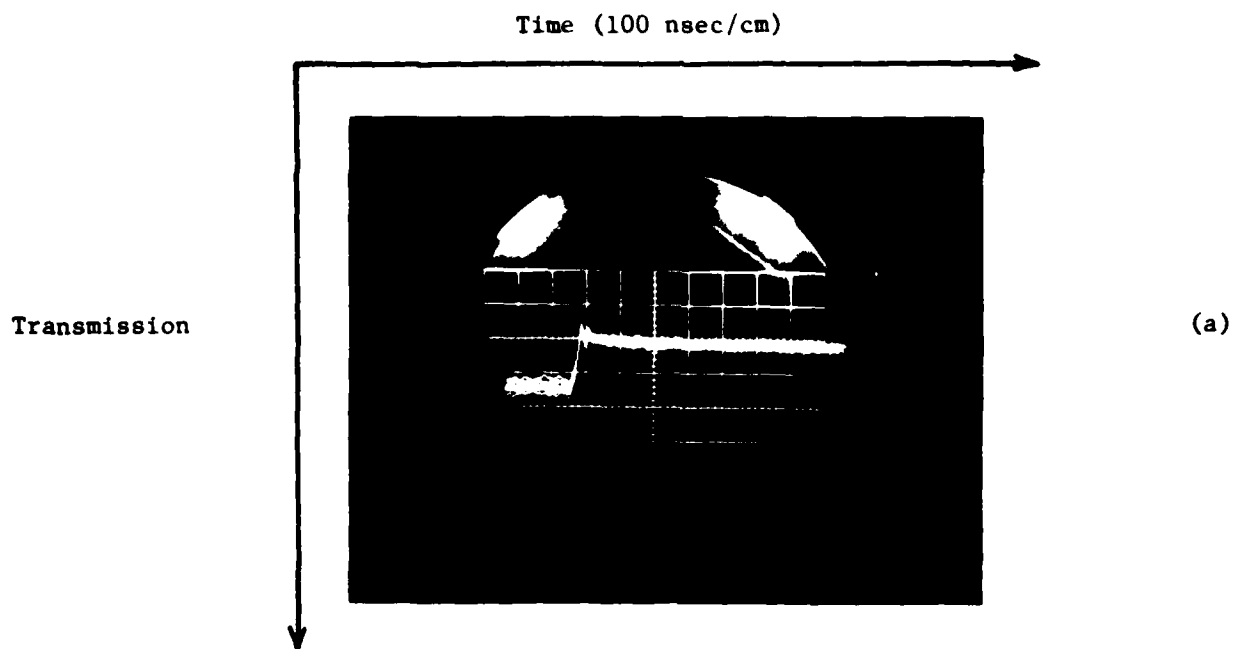
The long relaxation time of the excited state in OG-530 filter glass makes that material unacceptable for application in a fast optical switch. Because all of the other glasses we examined had comparable relaxation times, we decided to replace the excited-state absorber with a true two-photon absorber in the interferometer cavity. For the pump pulses of ~ 10 nsec duration used in this experiment, the turn on and turn off times of the switch will then be largely determined by the pump pulse duration, although for shorter pulses, the interferometer lifetime (≤ 1 ns for a 1 cm cavity) would become the limiting factor on the switching speed.

Cadmium sulfide is known to be a good two-photon absorber and is attractive in this application because it is transparent to the HeNe signal laser and nearly transparent to the SHG Nd:YAG pump radiation ($\alpha_{532} = .44 \text{ cm}^{-1}$). Although many measurements have been made of the two-photon absorption coefficient (β) for CdS, agreement among the reported values is not good, and no determinations have been made for the wavelengths used in our work. Therefore, we have made a rough measurement of β using the 532.0 nm pump and 632.8 nm signal beams ($\omega_p + \omega_s = 4.29 \text{ eV}$) with an experimental arrangement identical to that shown in Fig. 7. We find that $\beta = .4 + .2 \text{ MW/cm}^2$, which is higher than indicated by a recent series of measurements²⁰ ($\omega_{2\text{-photon}} = 3.18, 3.56, 3.91 \text{ eV}$), but may reflect an enhancement due to the proximity of the pump wavelength to the absorption edge of the crystal. We have also

measured the linear loss of our sample at Brewster's angle and find that $\alpha_o = .08 \text{ cm}^{-1}$ for an optical path length of 0.54 cm. Thus, for a cavity finesse of 15, we expect a 1 MW/cm^2 pulse to cause the interferometer transmission to decrease to about 50% of its initial value. At this intensity level there is little danger of causing optically induced damage to the CdS crystal.

With the 5 mm thick CdS crystal in the interferometer cavity at Brewster's angle, the measured transmission was $\sim 10\%$ and the finesse was ~ 15 . The linear absorption is too low to account for such poor transmission, which we therefore attribute to phase distortion of the signal beam due to the poor optical quality of the crystal (CdS is very soft and therefore difficult to polish to flat, scratch-free surfaces). Experimentally, we found that the CdS caused strong switching behavior for input intensities that were much too low to induce significant true two-photon absorption. In Fig. 12(a) the pump pulse has caused the transmission to drop to 32% of its initial value for an input intensity of 2 MW/cm^2 . Although we have estimated that this intensity should be able to cause significant two-photon absorption, we find that the single-pass loss induced for a pump intensity of 5.6 MW/cm^2 is only $\sim 7\%$, which is much too low to account for large changes in transmission with the cavity present. This apparent disagreement with our measured value of β is due to poor overlap of the pump and signal beams in the crystal when it is in the cavity. Also noteworthy in Fig. 12(a) is the long recovery time of the transmission. The pump pulse duration is only

FIGURE 12



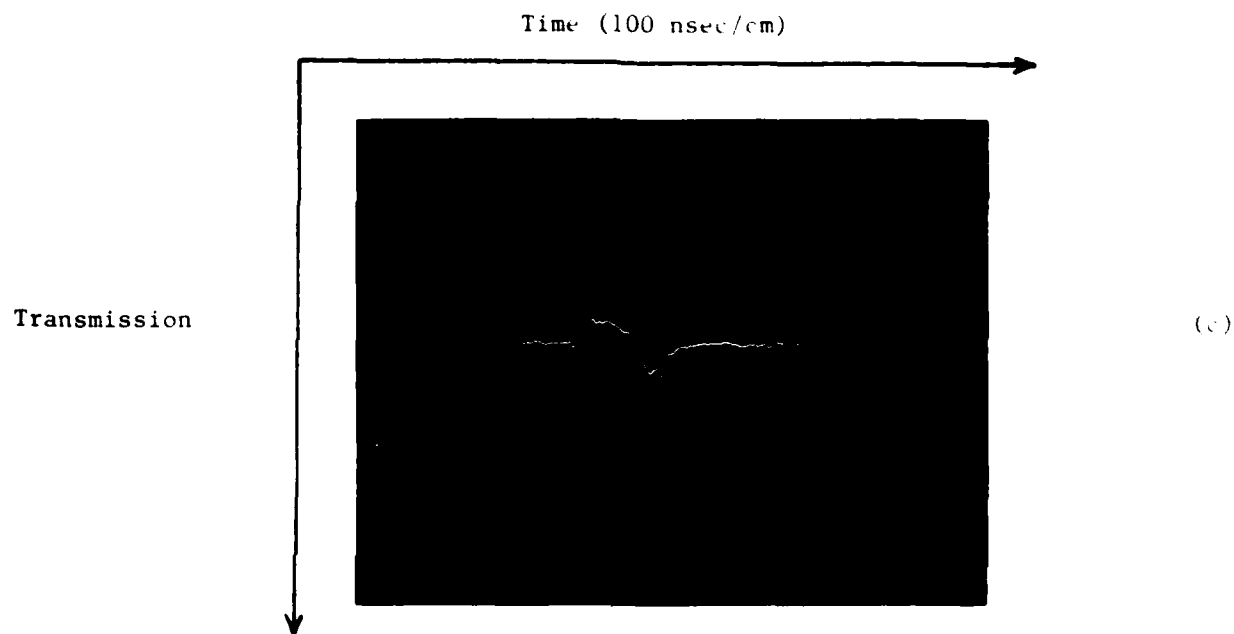


FIGURE 12. Pump induced change in transmission of a Fabry-Perot interferometer with intracavity CdS crystal for different pump energies and different initial cavity tuning. Pump energy densities are: (a) 11.0 mJ/cm^2 ; (b) 39.8 mJ/cm^2 ; and (c) 95.5 mJ/cm^2 .

10 nsec, but during the 70 nsec shown in the photograph following the pulse, the transmission increases only slightly toward its original level [although 100 ms later, when the next pump pulse is fired, the transmission has fully recovered; note that many successive traces are shown in Fig. 12(a)]. Figures 12(b) and (c) show the etalon transmission for higher pump powers and different initial cavity tuning. In both cases, the cavity is initially tuned for partial transmission, and the pump pulse induces a sharp decrease in T. During the relaxation period after the pulse, the transmission increases to the fully 'on' state in (b), and then cycles through the fully transmitting state back down to the initial transmission in (c). In both cases, the transmission fully recovers to its initial value before the next pump pulse (100 ms). Simply by changing the initial cavity tuning, it is possible to obtain waveforms similar to any of those shown in Fig. 12, as well as waveforms that show an initial, sharp increase in transmission.

This behavior can be understood with the aid of Fig. 13, in which the interferometer transmission is plotted as a function of the optical length within the cavity (which can be varied by changing the cavity spacing d or the crystal index of refraction n). In Fig. 13(a) the process responsible for the behavior shown in Fig. 12(a) is indicated. The cavity is initially tuned to point A by piezoelectrically varying the cavity spacing (d). The pump pulse then causes a rapid index change (step function proportional to the laser energy) which tunes the cavity to point B, a transmission minimum. As the index slowly recovers

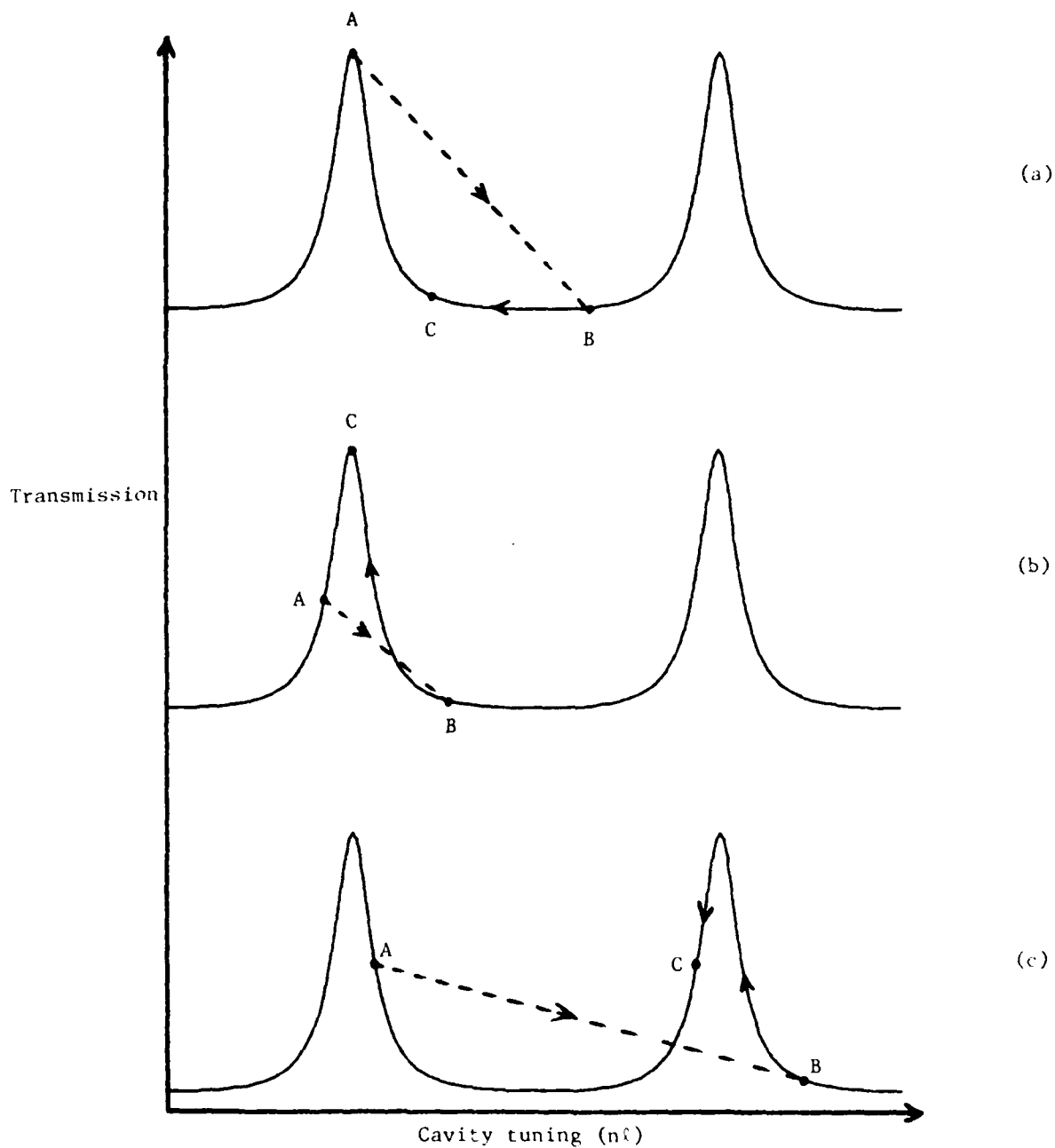


FIGURE 13. Explanation of the interferometer transmission behavior observed in Fig. 12 due to pump induced index change in intracavity CdS crystal. (a), (b), and (c) correspond to 12(a), 12(b), and 12(c), respectively. In all cases, A is the tuning of the cavity prior to the pump pulse, B is the tuning immediately after the pulse, and C is the tuning at the end of the traces shown in Fig. 12 (≈ 70 nsec after the pump pulse).

toward its initial value, the transmission does not increase until the cavity tuning recovers past point C, which requires a longer time than is shown in Fig. 12(a). Figure 13(b) explains the behavior observed in Fig. 12(b). The cavity is manually tuned to point A, and the pump induced index change retunes the cavity to point B. As the index recovers toward its initial value, the transmission moves along the tuning curve to a maximum at point C [this is the situation at the end of the oscilloscope trace shown in Fig. 12(b)]. When the pump pulse initially induces the index change, the transmission must also follow the tuning curve on its way from A to B, but no transmission peak is observed because the response of our oscilloscope is inadequate to resolve the peak produced by tuning from A through C to B in 10 ns. Figure 13(c) corresponds to Fig. 12(c) and is interpreted as in (a) and (b) above; the only difference is that the initial index change is greater because the pump energy is greater in this case. As before, point A represents the cavity tuning before the pump pulse, B represents the tuning immediately after the pulse, and C is the tuning at the end of the trace shown in the photograph (~ 70 ns after the pulse).

C. Discussion of Experimental Results - Induced Index Change

Although the experimental results shown so far for the intracavity filter glass and CdS crystal unambiguously indicate that the pump induced transmission change is due to a change in index rather than in absorption, the mechanism for this index change remains unresolved. The two most plausible mechanisms are that: (1) the index change is thermally induced by the 532.0 nm light absorbed by the sample; and (2) the index change is due to the population of excited electronic states by the absorbed pump radiation. We have verified that the mechanism is dependent on the absorption of the pump radiation by shifting the pump wavelength to the red where neither OG-530 glass or CdS is strongly absorbing (recall that 532.0 nm is near the absorption edge of OG-530 and CdS). The results of this experiment are given in Table 8, where the parameter η is defined as the ratio of pump energy density (mJ/cm^2) to induced change in interferometer transmission (% of maximum transmission). The increase in η for the two materials as λ_p moves to longer wavelengths indicates that higher input energy densities are required to induce a given transmission change as the linear absorption at ω_p decreases.

TABLE 8						
	λ_p (nm)	=	532.	565.	600.	620.
OG-530*	η (mJ/cm ²)	=	29.	62	361	1100
CdS**	η (mJ/cm ²)	=	26.			91
*for OG-530, finesse ~ 20						
**for CdS, finesse ~ 10						

We have made estimates of the magnitude of the index changes for which each of the two mechanisms may account and compared these numbers with the estimated index change required for the effects we observe. The transmission of an interferometer as a function of the index tuning away from resonance (δn) is:

$$T(\delta n) = \frac{1}{1 + F \sin^2 \left(\frac{2\pi \delta n \ell}{\lambda} \right)} .$$

This is solved to yield

$$\delta n/n = \frac{\lambda}{2\pi n \ell} \arcsin \left\{ \frac{1}{F} \left(\frac{1}{T} - 1 \right) \right\}^{1/2} .$$

From this we find that for an interferometer of finesse 15, a reduction of the transmission to 33% of its initial value requires an index change of $\delta n/n = 2.0 \times 10^{-6}$.

The thermally induced index change can be calculated from the known absorption of the material at 532.0 nm, its density, heat capacity, and its value of $\partial n/\partial T$. These values are known in the case of CdS and are listed in Table 9.²¹

TABLE 9	
Linear absorption, $\alpha_{532.}$	$= .44 \text{ cm}^{-1}$
Heat capacity, C_p	$= .080 \text{ cal/gm} - ^\circ\text{K}$
Density, ρ	$= 4.82 \text{ gm/cm}^3$
Refractive index change with temperature, $\partial n/\partial T$	$= 1.0 \times 10^{-4}/\text{K}$

In Fig. 12(a) the switch transmission is reduced to $\sim 32\%$ of its initial value by a pump pulse of energy density 11.0 mJ/cm^2 . Of the 80% of the energy transmitted by the crystal surface, 20% is absorbed over the 5 mm thickness of the crystal, causing a temperature increase in the illuminated region of $2.1 \times 10^{-3} \text{ K}$. This temperature increase causes an index change of $\delta n/n = 8.7 \times 10^{-8}$, a factor of 20 times smaller than that estimated to be necessary to produce a transmission of 33%.

The magnitude of the index change produced by the population redistribution mechanism can be crudely estimated from a free electron model in which the dielectric constant at ω_s is written as

$$\epsilon(\omega_s) = \epsilon_{\text{bound}} + 1 - (\omega_{pl}/\omega_s)^2,$$

where $(\epsilon_{\text{bound}} + 1)$ is the contribution due to bound electrons and free space, and $-(\omega_{pl}/\omega_s)^2$ is the contribution due to the free carriers created by the absorbed pump photons. The plasma frequency, ω_{pl} , is given by

$$\omega_{pl}^2 = \frac{4\pi N e^2}{m^*}$$

where N = density of photo-induced free carriers

m^* = effective mass of the free carriers.

If we assume that initially $N = 0$, the index change is simply due to the free carriers created by the pump, and

$$\frac{\delta n}{n} = \frac{2\pi N e^2}{m n \omega_s^2} .$$

Again for an incident energy density of 11.0 mJ/cm^2 , we find that $N = 9.3 \times 10^{15} \text{ cm}^{-3}$, which results in $\delta n/n = 1.3 \times 10^{-6}$. Although this index change is very close to the index change estimated necessary to cause $T = 33\%$, it is almost certainly an overestimate, since this simple free electron model has ignored the effect of trapped states which will tend to decrease the number of free carriers.

We have also estimated the relaxation time of a thermal or free carrier induced change in the refractive index of CdS. From three-photon induced conductivity experiments, Jayaraman and Lee²² have found that the conductivity decay in CdS exhibits three distinct regions: (1) fast relaxation on the order of 1 μsec due to free carrier recombination and trap filling; (2) intermediate relaxation on the order of 35 μsec due to the release of electrons from traps; and (3) a very slow (\sim seconds) relaxation due to the emptying of low lying traps close to the equilibrium Fermi level. These relaxation times are not inconsistent with our results on CdS; however, we are unable to establish quantitative agreement because the apparent relaxation of the induced index change observed with CdS in the interferometer depends strongly on the initial cavity tuning. We are therefore unable to make an accurate measurement of the true relaxation time of the induced index change.

The relaxation time of a thermally induced index change can be roughly estimated by considering the simple problem of transient heat flow in an

infinite solid in one dimension. Assume that the pump laser induces a Gaussian-distributed high temperature region described by

$$T(x, t = 0) = T_0 e^{-x^2/A^2}$$

where T_0 = maximum initial temperature (at $x = 0$), and A = radius of the heated spot. By solving the transient heat flow equation in one dimension, one can show that the time behavior of the temperature at the spot center is

$$T(x = 0, t) = T_0 \frac{A}{(A^2 + 4\alpha t)^{1/2}} \quad (7)$$

where

α = thermal diffusivity = $k/\rho c_p$

k = thermal conductivity

ρ = density

c_p = heat capacity.

From Eq. (7) we find that the temperature decays away to one-half of its initial value after time $t_{1/2}$, where

$$t_{1/2} = \frac{3A^2}{4\alpha}$$

For CdS, $k = .2$ watts/cm-K,²¹ which yields $\alpha = .13$ cm²/sec. Thus we find that for CdS, $t_{1/2} = 58$ msec. Although this calculation was based on a one-dimensional model, this value of $t_{1/2}$ is probably correct to within an order of magnitude and does appear to be too long to account for the effects we have observed in CdS. However, our inability to accurately determine the index relaxation time makes it difficult to conclusively exclude the thermal mechanism from consideration.

In conclusion, we have observed strong switching of a Fabry-Perot interferometer with intracavity CdS and OG-530 glass for anomalously low pump intensities. Order of magnitude estimates of the required pump energies and of the relaxation time of the induced index change for two different mechanisms suggest that the index change is due to electronic rather than to thermal effects, but we are unable to conclusively identify the mechanism at this time.

VII. THE PHOTOREFRACTIVE EFFECT

We have conducted a computer-aided literature search in an effort to find materials that exhibit photo-induced changes in their refractive indices and are suitable for use in making photo-induced waveguides. (Appendix A contains a list of the pertinent papers uncovered in this search.) The criteria that a material must satisfy in order to be useful are that: (1) the induced index change must be positive; (2) the index change must be long-lived; (3) the index change must be sufficiently large; and (4) the refractive index of the material must approximately match the index of glass core fibers. The only attractive candidate material we have found is Ge-doped silica glass, which has been used in the core of optical fibers to construct Bragg reflectors.^{2,3}

The Ge-doped silica sample that we obtained from Bell Labs exhibits a striated structure that badly distorts the spatial distribution of transmitted light. We were unable to remove the structure by annealing the glass and therefore attempted to cut the sample so that light could be transmitted parallel to the striae without distortion. This was only partly successful, for although we were able to pass a laser beam through the sample, much of the light was scattered out of the central core of the beam.

We attempted to measure the photorefractive effect in Ge:SiO_2 by using a strong laser beam (Ar ion laser, $\lambda = 514.5 \text{ nm}$) to induce a waveguide directly into the bulk of the sample. A second, weaker beam (HeNe laser, $\lambda = 632.8 \text{ nm}$) is then used to probe for the existence of the induced channel. Initially, the two beams are crossed at an angle ϕ in

the homogeneous sample (see Fig. 14). If the strong beam does cause an index change, δn , the weak beam will be guided if θ ($\theta \approx 90^\circ - \phi$) exceeds the critical angle determined by the index change, thus resulting in an angular deflection of the weak beam. For a small index change δn , the critical angle θ_c is

$$\theta_c = \arcsin(1 - \delta n/n).$$

An induced index change of only 0.1% implies a critical angle $\theta_c = 87.4^\circ$, thus allowing an angular separation of the strong and weak beams of as much as 2.6° .

In our experiment, the two laser beams were crossed at an angle of $\phi = 0.5^\circ$ in the sample and were then projected onto a screen 60 cm away, where their separation was 0.5 cm; thus any angular deflection of the HeNe beam could easily be observed. The laser spot diameters at the sample were measured with a linear diode array to be 140 μ and 210 μ for the strong and weak beams, respectively. No permanent deviation of the weak beam was observed after a 100 sec exposure with a strong beam power of 1.5 Watts (9.7 kW/cm^2), although there was a very small temporary shift (0.1°) when the strong beam was present, probably due to thermal effects. For a crossing angle of $\phi = .5^\circ$, we would expect the probe beam to be guided for an index change of only $\delta n/n \approx 4 \times 10^{-5}$. Our inability to observe a deviation suggests that the poor optical quality of our sample may have inhibited the photorefractive effect, since this technique, which makes use of the total internal reflection between the illuminated core and the surrounding medium, should be quite sensitive.

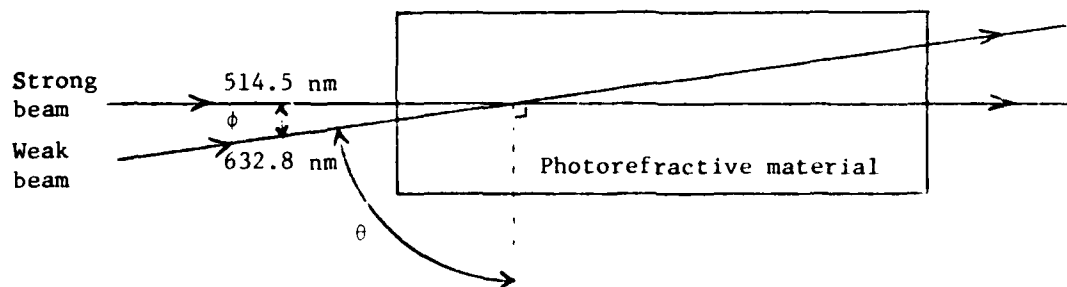


FIGURE 14. Experimental arrangement for measuring photorefractive effect.

REFERENCES

1. G. Mayer and F. Gires, "Action of an Intense Light Beam on the Refractive Index of Liquids," C.R. Acad. Sci. (France) 258, 2039 (1964).
2. P.D. Maker and R.W. Terhune, "Study of Optical Effects Due to an Induced Polarization Third Order in the Electric Field Strength," Phys. Rev. 137, 801 (1965).
3. A. Owyong, R.W. Hellwarth, and N. George, "Intensity-Induced Changes in Optical Polarizations in Glasses," Phys. Rev. B 5, 628 (1972).
4. G.K.L. Wong and Y.R. Shen, "Optical-Field-Induced Ordering in the Isotropic Phase of a Nematic Liquid Crystal," Phys. Rev. Lett. 30, 895 (1973).
5. M. Born and E. Wolf, Principles of Optics, 5th ed. (Pergamon Press, 1975), p. 325.
6. F.S. Felber and J.H. Marburger, "Theory of Nonresonant Multistable Optical Devices," Appl. Phys. Lett. 28, 731 (1976); J.H. Marburger and F.S. Felber, "Theory of a Lossless Nonlinear Fabry-Perot Interferometer," Phys. Rev. A 17, 335 (1978).
7. T. Bischofberger and Y.R. Shen, "Nonlinear Fabry-Perot Filled with CS₂ and Nitrobenzene," Opt. Lett. 4, 40 (1979).
8. P.D. Maker, R.W. Terhune, and C.M. Savage, "Intensity-Dependent Changes in the Refractive Index of Liquids," Phys. Rev. Lett. 12, 507 (1964).

9. P.D. McWane and D.A. Sealer, "New Measurements of Intensity-Dependent Changes in the Refractive Index of Liquids," Appl. Phys. Lett. 8, 278 (1966).
10. F.B. Martin and J.R. Lalanne, "Agreement between Depolarized Rayleigh Scattering and Optical Kerr Effect Induced by Q-Switched Laser Waves in Some Liquids," Phys. Rev. A 4, 1275 (1971).
11. H.J. Coles and B.R. Jennings, "Laser-Induced Birefringence in Pure Liquids," Philos. Mag. (GB) 32, 1051 (1975).
12. J.F. Giuliani and J. Van Laak, "Laser-Induced Birefringence in Polar Liquids," J. Opt. Soc. Am. 66, 372 (1976).
13. J.P. Hermann, D. Ricard, and J. Ducuing, "Optical Nonlinearities in Conjugated Systems: β -Carotene," Appl. Phys. Lett. 23, 178 (1973).
14. J.P. Hermann and J. Ducuing, "Third-Order Polarizabilities of Long-Chain Molecules," J. Appl. Phys. 45, 5100 (1974).
15. J.J. Wynne and G.D. Boyd, "Study of Optical Difference Mixing in Ge and Si Using a CO_2 Gas Laser," Appl. Phys. Lett. 12, 191 (1968).
16. E. Yablonovitch, C. Flytzanis, and N. Bloembergen, "Anisotropic Interference of Three-Wave and Double Two-Wave Frequency Mixing in GaAs," Phys. Rev. Lett. 29, 865 (1972).
17. S.D. Kramer, F.G. Parsons, and N. Bloembergen, "Interference of Third-Order Light Mixing and Second-Harmonic Exciton Generation in CuCl_2 ," Phys. Rev. B 9, 1853 (1974).
18. D. Heiman, R.W. Hellwarth, M.D. Levenson, and G. Martin, "Raman-Induced Kerr Effect," Phys. Rev. Lett. 36, 189 (1976).

19. J.J. Song and M.D. Levenson, "Electronic and Orientational Contributions to the Optical Kerr Constant Determined by Coherent Raman Techniques," *J. Appl. Phys.* 48, 3496 (1977).
20. C. B. de Araujo and H. Lotem, "New Measurements of the Two-Photon Absorption in GaP, CdS, and ZnSe Relative to Raman Cross Sections," *Phys. Rev. B* 18, 30 (1978).
21. Linear absorption, α_{532} , measured in this work. Other material constants from M. Neuberger, II-VI Semiconducting Compounds Data Tables, Electronic Properties Information Center (1969).
22. S. Jayaraman and C.H. Lee, "Observation of Three-Photon Conductivity in CdS with Mode-Locked Nd:glass Laser Pulses," *J. Appl. Phys.* 44, 5480 (1973).
23. K.O. Hill, Y. Fujii, D.C. Johnson, and B.S. Kawasaki, "Photosensitivity in Optical Fiber Waveguides: Application to Reflection Filter Fabrication," *Appl. Phys. Lett.* 32, 647 (1978); B.S. Kawasaki, K.O. Hill, D.C. Johnson, and Y. Fujii, "Narrow-Band Bragg Reflectors in Optical Fibers," *Opt. Lett.* 3, 66 (1978).

APPENDIX A

BIBLIOGRAPHY ON THE PHOTOREFRACTIVE EFFECT

GENERAL

1. J.J. Amodei, W. Phillips, and D.L. Staebler, "Improved Electrooptic Materials and Fixing Techniques for Holographic Recording," Appl. Opt. 11, 390 (1972).
2. A.M. Glass, "The Photorefractive Effect," Opt. Eng. 17, 470 (1978).
3. F. Micheron, "Sensitivity of the Photorefractive Processes," Ferroelectrics 18, 153 (1978).
4. D. von der Linde and A.M. Glass, "Photorefractive Effects for Reversible Holographic Storage of Information," Appl. Phys. 8, 85 (1975).

POTASSIUM TANTALATE NIOBATE (KTN)

1. F.S. Chen, "A Laser-Induced Inhomogeneity of Refractive Indices in KTN," J. Appl. Phys. 38, 3418 (1967).
2. D. von der Linde, A.M. Glass, and K.F. Rodgers, "High-Sensitivity Optical Recording in KTN by Two-Photon Absorption," Appl. Phys. Lett. 26, 22 (1975).

CADMIUM SULFIDE (CdS)

1. A. Ashkin, B. Tell, and J.M. Dziedzic, "Laser Induced Refractive Index Inhomogeneities and Absorption Saturation Effects in CdS," IEEE J. Quantum Electron. QE-3, 400 (1967).

BISMUTH TITANATE ($\text{Bi}_4\text{Ti}_3\text{O}_{12}$) AND BARIUM TITANATE (BaTiO_3)

1. L.H. Lin, "Holographic Measurements of Optically Induced Refractive Index Inhomogeneities in Bismuth Titanate," Proc. IEEE 57, 252 (1969).
2. F. Micheron and G. Bismuth, "Electrical Control of Fixation and Erasure of Holographic Patterns in Ferroelectric Materials," Appl. Phys. Lett. 20, 79 (1972).
3. R.L. Townsend and J.T. LaMacchia, "Optically Induced Refractive Index Changes in BaTiO_3 ," J. Appl. Phys. 41, 5188 (1970).

STRONTIUM BARIUM NIOBATE (SBN) AND BARIUM SODIUM NIOBATE ($\text{Ba}_2\text{NaNb}_5\text{O}_{15}$)

1. J.J. Amodei and D.L. Staebler, "Holographic Pattern Fixing in Electro-Optic Crystals," Appl. Phys. Lett. 18, 540 (1971).
2. J.J. Amodei, D.L. Staebler, and A.W. Stephens, "Holographic Storage in Doped Barium Sodium Niobate ($\text{Ba}_2\text{NaNb}_5\text{O}_{15}$)," Appl. Phys. Lett. 18, 507 (1971).
3. A.V. Guinzberg, K.D. Kochev, Yu.S. Kusminov, and T.R. Volk, "The Photoferroelectric Mechanism of the Effect of 'Optical Damage' in Strontium Barium Niobate Crystals," Phys. Stat. Sol. (a) 29, 309 (1975).
4. J.B. Thaxter, "Electrical Control of Holographic Storage in Strontium-Barium Niobate," Appl. Phys. Lett. 15, 210 (1969).
5. J.B. Thaxter and M. Kestigian, "Unique Properties of SBN and Their Use in a Layered Optical Memory," Appl. Opt. 13, 913 (1974).

CHALCOGENIDE GLASS (As-Se-S-Ge)

1. T. Igo and Y. Toyoshima, "A Reversible Optical Change in the As-Se-Ge Glass," J. Non-Cryst. Solids 11, 304 (1973).
2. O. Mikami, J. Noda, S. Zembutsu, and S. Fukunishi, "Phase Tuning in Optical Directional Coupler by Photostructural Effect of Chalcogenide Glass Film," Appl. Phys. Lett. 31, 376 (1977).
3. S. Zembutsu and S. Fukunishi, "Waveguiding Properties of (Se,S)-based Chalcogenide Glass Films and Some Applications to Optical Waveguide Devices," Appl. Opt. 18, 393 (1979).
4. S. Zembutsu, Y. Toyoshima, T. Igo, and H. Nagai, "Properties of (Se,S)-based Chalcogenide Glass Films, and an Application to a Holographic Supermicrofiche," Appl. Opt. 14, 3073 (1975).

LEAD-LANTHANUM TITANO-ZIRCONATE CERAMICS (PLZT)

1. J.W. Burgess, R.J. Hurditch, C.J. Kirkby, and G.E. Scrivener, "Holographic Storage and Photoconductivity in PLZT Ceramic Materials," Appl. Opt. 15, 1550 (1976).
2. F. Micheron, C. Mayeux, and J.C. Trotier, "Electrical Control in Photoferroelectric Materials for Optical Storage," Appl. Opt. 13, 784 (1974).

BISMUTH SILICATE AND BISMUTH GERMANATE (BSO AND BGO)

1. J.P. Huignard and J.P. Herriau, "Real-time Double-exposure Interferometry with $\text{Bi}_{12}\text{SiO}_{20}$ Crystals in Transverse Electrooptic Configuration," Appl. Opt. 16, 1807 (1977).

2. J.P. Huignard and F. Micheron, "High-sensitivity Read-Write Volume Holographic Storage in $\text{Bi}_{12}\text{SiO}_{20}$ and $\text{Bi}_{12}\text{GeO}_{20}$ Crystals," Appl. Phys. Lett. 29, 591 (1976).
3. M. Peltier and F. Micheron, "Volume Hologram Recording and Charge Transfer Process in $\text{Bi}_{12}\text{SiO}_{20}$ and $\text{Bi}_{12}\text{GeO}_{20}$," J. Appl. Phys. 48, 3683 (1977).

Ge-DOPED SILICA GLASS

1. K.O. Hill, Y. Fujii, D.C. Johnson, and B.S. Kawasaki, "Photosensitivity in Optical Fiber Waveguides: Application to Reflection Filter Fabrication," Appl. Phys. Lett. 32, 647 (1978).
2. K.O. Hill, B.S. Kawasaki, D.C. Johnson, and Y. Fujii, "Nonlinear Effects in Optical Fibers: Application to the Fabrication of Active and Passive Devices" (to be published).
3. B.S. Kawasaki, K.O. Hill, D.C. Johnson, and Y. Fujii, "Narrow-band Bragg Reflectors in Optical Fibers," Opt. Lett. 3, 66 (1978).

LITHIUM TANTALATE (LiTaO_3) AND LITHIUM NIOBATE (LiNbO_3)

1. A. Ashkin, G.D. Boyd, J.M. Dziedzic, R.G. Smith, A.A. Ballman, J.J. Levinstein, and K. Nassau, "Optically-Induced Refractive Index Inhomogeneities in LiNbO_3 and LiTaO_3 ," Appl. Phys. Lett. 9, 72 (1966).
2. C-T Chen, D.M. Kin, and D. von der Linde, "Efficient Hologram Recording in $\text{LiNbO}_3:\text{Fe}$ Using Optical Pulses," Appl. Phys. Lett. 34, 321 (1979).

3. F.S. Chen, "Optically Induced Change of Refractive Indices in LiNbO_3 and LiTaO_3 ," J. Appl. Phys. 40, 3389 (1969).
4. F.S. Chen, J.T. LaMacchia, and D.B. Fraser, "Holographic Storage in Lithium Niobate," Appl. Phys. Lett. 13, 223 (1968).
5. M.G. Clark, F.J. DiSalvo, A.M. Glass, and G.E. Peterson, "Electronic Structure and Optical Index Damage of Iron-Doped Lithium Niobate," J. Chem. Phys. 59, 6209 (1973).
6. W.D. Cornish and L. Young, "Influence of Multiple Internal Reflections and Thermal Expansion on the Effective Diffraction Efficiency of Holograms Stored in Lithium Niobate," J. Appl. Phys. 46, 1252 (1975).
7. W.D. Cornish, M.G. Moharam, and L. Young, "Effects of Applied Voltage on Hologram Writing in Lithium Niobate," J. Appl. Phys. 47, 1479 (1976).
8. B. Dischler, J.R. Herrington, A. Räuber, and H. Kurz, "Correlation of the Photorefractive Sensitivity in Doped LiNbO_3 with Chemically Induced Changes in the Optical Absorption Spectra," Solid State Commun. 14, 1233 (1974).
9. A.M. Glass, D. von der Linde, and T.J. Negran, "High-voltage Bulk Photovoltaic Effect and the Photorefractive Process in LiNbO_3 ," Appl. Phys. Lett. 25, 233 (1974).
10. A. Ishida, O. Mikami, S. Miyazawa, and M. Sumi, "Rh-doped LiNbO_3 as an Improved New Material for Reversible Holographic Storage," Appl. Phys. Lett. 21, 192 (1972).
11. W.D. Johnston, Jr., "Optical Index Damage in LiNbO_3 and Other Pyroelectric Insulators," J. Appl. Phys. 41, 3279 (1970).

12. H. Kurz, E. Krätzig, W. Keune, H. Engelmann, U. Gonser, B. Dischler, and A. Räuber, "Photorefractive Centers in LiNbO_3 , Studied by Optical-, Mössbauer- and EPR-Methods," Appl. Phys. 12, 355 (1977).
13. J. Noda, S. Zembutsu, S. Fukunishi, and N. Uchida, "Strip-loaded Waveguide Formed in a Graded-index LiNbO_3 Planar Waveguide," Appl. Opt. 17, 1953 (1978).
14. G.E. Peterson, A.M. Glass, and T.J. Negran, "Control of the Susceptibility of Lithium Niobate to Laser-Induced Refractive Index Changes," Appl. Phys. Lett. 19, 130 (1971).
15. W. Phillips, J.J. Amodei, and D.L. Staebler, "Optical and Holographic Storage Properties of Transition Metal Doped Lithium Niobate," RCA Rev. 33, 94 (1972).
16. J.M. Spinhirne, D. Ang, C.S. Joiner, and T.L. Estle, "Simultaneous Holographic and Photocurrent Studies of the Photorefractive Effect in LiTaO_3 and LiNbO_3 ," Appl. Phys. Lett. 30, 89 (1977).
17. D.L. Staebler, W.J. Burke, W. Phillips, and J.J. Amodei, "Multiple Storage and Erasure of Fixed Holograms in Fe-doped LiNbO_3 ," Appl. Phys. Lett. 26, 182 (1975).
18. D.L. Staebler and W. Phillips, "Fe-doped LiNbO_3 for Read-Write Applications," Appl. Opt. 13, 788 (1974).
19. H. Tsuya, "Optical Damage in Transition-Metal-Doped LiTaO_3 ," J. Appl. Phys. 46, 4323 (1975).
20. C.M. Verber, N.F. Hartman, and A.M. Glass, "Formation of Integrated Optics Components by Multiphoton Photorefractive Processes," Appl. Phys. Lett. 30, 272 (1977).

21. D. von der Linde, A.M. Glass, and K.F. Rodgers, "Multiphoton Photo-refractive Processes for Optical Storage in LiNbO_3 ," Appl. Phys. Lett. 25, 155 (1974).
22. D. von der Linde, A.M. Glass, and K.F. Rodgers, "Optical Storage Using Refractive Index Changes Induced by Two-step Excitation," J. Appl. Phys. 47, 217 (1976).
23. D. von der Linde, O.F. Schirmer, and H. Kurz, "Intrinsic Photo-refractive Effect of LiNbO_3 ," Appl. Phys. 15, 153 (1978).
24. V.E. Wood, N.F. Hartman, C.M. Verber, and R.P. Kenan, "Holographic Formation of Gratings in Optical Waveguiding Layers," J. Appl. Phys. 46, 1214 (1975).
25. L. Young, W.K.Y. Wong, M.L.W. Thewalt, and W.D. Cornish, "Theory of Formation of Phase Holograms in Lithium Niobate," Appl. Phys. Lett. 24, 264 (1974).



MISSION of Rome Air Development Center

RADC plans and executes research, development, test and selected acquisition programs in support of Command, Control Communications and Intelligence (C³I) activities. Technical and engineering support within areas of technical competence is provided to ESD Program Offices (POs) and other ESD elements. The principal technical mission areas are communications, electromagnetic guidance and control, surveillance of ground and aerospace objects, intelligence data collection and handling, information system technology, ionospheric propagation, solid state sciences, microwave physics and electronic reliability, maintainability and compatibility.

END

DATE
FILMED

5 - 8 - 1

DTIC